Early antigen receptor signaling in natural killer cells alters STAT4-dependent fate decisions via epigenetic remodeling

Simon Grassmann*[,1], Endi K. Santosa*[,1,2], Adriana M. Mujal[1], Hyunu Kim[1], Sherry X. Fan[1], Mark Owyong[1,2], Colleen M. Lau[3], Joseph C. Sun[1,2]

[1]Immunology Program, Memorial Sloan Kettering Cancer Center, New York, NY, USA
[2]Department of Immunology and Microbial Pathogenesis, Weill Cornell Medical College, New York, NY USA
[3]Department of Microbiology and Immunology, Cornell University College of Veterinary Medicine

Correspondence:
Simon Grassmann, MD
Memorial Sloan Kettering Cancer Center
408 East 69th Street, ZRC-1462
New York, NY 10065
Phone: 646-888-3228
Email: grassmas@mskcc.org

Joseph C. Sun, PhD
Memorial Sloan Kettering Cancer Center
408 East 69th Street, ZRC-1462
New York, NY 10065
Phone: 646-888-3228
Email: sunj@mskcc.org

ABSTRACT

Natural Killer (NK) cells are innate cytotoxic lymphocytes that possess features of adaptive immunity, including antigen specificity and clonal expansion. NK cells rapidly respond to cytokines released during the innate phase of viral infection and are thought to migrate from circulation into infected organs to execute their early effector functions. However, recent evidence suggests that tissue-resident NK cells are among the first responders to viral infection. In this study, we observe that antigen receptor signaling precedes substantial proinflammatory cytokine signaling in a population of NK cells during mouse cytomegalovirus infection. Early antigen receptor signals epigenetically prime NK cells for optimal expansion during the later adaptive phase of the antiviral response. Mechanistically, receptor signaling increases chromatin accessibility at STAT4-binding genomic sites within differentiating NK cells. To promote adaptive programming of NK cells during infection, activating receptor-dependent epigenetic remodeling antagonizes IL-12 driven terminal maturation, poises NK cells for proliferation via sustained CDK6 expression, and antagonizes early apoptosis of short-lived effector cells via suppression of Bim. Thus, antigen receptor signaling alters an IL-12 dependent fate decision during the innate-to-adaptive transition of antiviral NK cells.

INTRODUCTION

Natural Killer (NK) cells are lymphocytes of the innate immune system. During virus infection, NK cells receive cytokine signals and serve as early immune effector cells by releasing interferon-gamma (IFN-γ) and directly killing virus-infected cells via activating receptors. Following the early innate phase of infection, NK cells are also capable of clonal expansion during various infections such as cytomegalovirus[1-3]. For such adaptive responses to occur, NK cells recognize viral antigen via activating receptors such as Ly49H in mice[4-6]. However, the precise sequence by which NK cells execute their innate and adaptive functions, and whether the same NK cells similarly participate in both, is incompletely understood.

Because NK cells are predominantly considered circulating lymphocytes, they are thought to be recruited to the site of infection via chemokines and cytokines released by myeloid and dendritic cells[7,8]. However, recent studies have demonstrated that NK cells comprise both circulating and tissue resident subsets[9]. During mouse cytomegalovirus (MCMV) infection, a population of splenic Ly49H$^+$ NK cells with an ILC1-like phenotype are tissue-resident and rapidly form antigen-specific NK cell-DC clusters immediately after infection[10]. In salivary glands, circulating NK cells can also differentiate into resident memory cells following infection[11]. Whether such tissue-resident NK cells first recognize virus-infected cells through antigen receptors before encountering proinflammatory cytokines remains unclear.

In this study, we sought to better understand the sequence of early events that occur during virus infection. We observed that NK cells receive antigen receptor signals prior to substantial cytokine signals during MCMV infection. These early antigen-

experienced NK cells were poised for optimal clonal expansion, showing enhanced proliferation. Mechanistically, epigenetic remodeling mediated by antigen receptor signaling was revealed by increased chromatin accessibility at binding sites for the transcription factor STAT4 downstream of the IL-12 receptor. In addition, activating receptor signals directly modulate H3K4 methylation at STAT4-dependent genes. In the absence of antigen receptor signaling, IL-12 instead drove an innate effector fate in NK cells characterized by terminal maturation and diminished proliferation. Thus, antigen receptor-dependent epigenetic remodeling antagonizes IL-12-driven terminal maturation of NK cells, and poises them for clonal expansion by promoting sustained CDK6 expression and suppressing expression of the apoptosis regulator Bim *in vitro* and *in vivo*, facilitating fate programming as NK cells transition from innate to adaptive states.

RESULTS

Early antigen receptor signaling precedes substantial cytokine signaling in NK cells during MCMV infection

To characterize the early response of NK cells to MCMV infection, we sorted NK cells from spleens of infected mice on days 1, 2, 3, and 4 post infection (PI) and performed single cell RNA-sequencing (scRNAseq) (**Fig. 1A**). To identify the earliest transcriptional changes of NK cells reacting to MCMV, we performed Louvain clustering and plotted the proportion of single-cell transcriptomes derived from NK cells at different time points within each cluster (**Fig. 1B**). Although clusters 0, 1, 3 and 9 were all enriched for day 1 PI, only cluster 9 (highlighted by dotted circle) was not simultaneously enriched for transcriptomes from uninfected mice. For a more thorough analysis, we focused on differentially expressed (DE) genes from day 1 PI, and Louvain clustering revealed a cluster reminiscent of cluster 9 in the pooled analysis, highlighted by dotted circle as cluster 4 (**Fig. 1C** and **Supp. Fig. 1**). *Klra8*, the gene encoding for the antigen receptor Ly49H in NK cells was among the top enriched genes in this cluster. Apart from the chemokines *Ccl3*, *Ccl4* and *Xcl1*, several of the top DE genes of this cluster were known to be those induced by antigen receptor signaling, such as Nr4a and Egr family members[12-14]. Expression of these genes appeared to be specifically enriched in early responding NK cells found in cluster 4 (**Fig. 1D**). Enrichment of such antigen-receptor dependent genes led us to hypothesize that antigen receptor signaling precedes other signals received by NK cells during MCMV infection. To substantiate this hypothesis, we incorporated a published cytokine signaling score versus an antigen-receptor signaling score derived from RNA-seq of NK cells stimulated with activating receptors, and

evaluated expression of the respective sets of DE genes compared to our dataset (**Fig. 1E**). Whereas NK cells on day 2 PI showed a strong expression of cytokine-dependent genes, NK cells found in cluster 9 were best characterized by antigen-receptor signaling, and only found at day 1 PI. Thus, antigen-receptor signaling appears to precede substantial cytokine signaling in the earliest NK cells reacting to MCMV infection.

Early antigen receptor signaling primes the clonal expansion of NK cells

Among the genes upregulated on day 1 PI was *Nr4a1*, a well-known target of antigen receptor signaling[12]. To investigate NK cells that received early antigen signaling in more detail, we made use of a Nr4a1 (Nur77) GFP reporter mouse[15]. Confirming the scRNAseq kinetic, Ly49H$^+$ NK cells upregulated Nur77-GFP on day 1 PI (**Fig. 2A**), and expression of Nur77-GFP was sustained to day 2 PI, compared to uninfected controls (**Fig. 2B**). By day 3 PI, GFP expression returned to levels observed in uninfected mice. In prior studies, MCMV-infected cells were found earlier in the spleen than in the liver[16], and we similarly observed that the earliest Nur77-GFP signals appearing on day 1 PI occurred in the spleen, but not blood or liver (**Fig. 2C** and **2D**).

Previously, we showed that spleen-resident NK cells with an ILC1-like phenotype recognize MCMV-infected cells on day 1 PI[10]. Indeed, when segregating the Ly49H$^+$ NK cells on day 1 PI into Nur77^{high} and Nur77^{low} subsets, the spleen-resident NK cells (characterized as CD27$^+$ CD62L$^-$) were only found among the Nur77^{high} population (**Fig. 2E** and **2F**). Overall, however, only 5-10% of the Nur77^{high} subset had the resident NK phenotype, suggesting both circulating and tissue-resident Ly49H$^+$ NK cells can receive

this early antigen signal. The major difference between Nur77^{high} and Nur77^{low} NK cells was an enrichment of CD27^{+} subsets in Nur77^{high} NK cells (**Fig. 2E** and **2F**).

Next, we tested whether the early antigen-receptor signal affected subsequent clonal expansion of different Ly49H^{+} NK cell populations based on Nur77-GFP expression. To directly compare the expansion potential of antigen-experienced (Nur77^{high}) and unexperienced (Nur77^{low}) NK cells, we infected Nur77-GFP mice expressing distinguishable congenic markers and sorted Ly49H^{+} NK cells with high or low GFP expression on day 1 PI (**Fig. 2G**). To ensure that differences in maturation states did not affect the experiment, we sorted only NK cells positive for CD27. We co-transferred these cells into infection-matched *Ly49h*$^{-/-}$ mice and observed that Nur77^{high} NK cells showed greater expansion than Nur77^{low} NK cells (**Fig. 2G**). Altogether, our findings suggest early antigen-receptor signaling is crucial for optimal clonal expansion following MCMV infection.

Early antigen receptor signaling is the dominant driver of transcriptional and epigenetic changes

Although the DE genes identified in early antigen-experienced NK cells from the scRNAseq time course best describe antigen receptor signaling, Nur77^{high} Ly49H^{+} NK cells on day 1 PI may also receive proinflammatory cytokine signals. To test this, we performed RNA-seq and ATAC-seq of Ly49H^{-}, Ly49H^{+} Nur77^{high} and Ly49H^{+} Nur77^{low} NK cells on day 1 PI (**Fig. 3A** and **3B**). (To eliminate effects due to maturation, Ly49H^{-} NK cells were sorted for positivity of Ly49D, a related activating receptor that can bind to certain MHC molecules, but does not recognize MCMV[17].) Nur77^{high} Ly49H^{+} NK cells

showed a transcriptional profile and epigenome distinct from both Nur77^{low} Ly49H^{+} NK cells and Ly49H^{-} NK cells (**Fig. 3C** and **3D**).

Interestingly, early antigen experienced NK cells appeared to show increased chromatin accessibility in exonic, intergenic, and particularly intronic regions, while accessibility in promoter regions decreased globally (**Fig. 3E** and **Supp. Fig. 2A**). From this dataset, we tested whether early antigen-experienced NK cells also showed evidence of cytokine signaling. IL-12, type 1 IFNs, IL-2 and IL-15 are rapidly produced and peak at around day 2 PI[18]. We compared RNA-seq and ATAC-seq data from antigen-experienced Nur77^{high} NK cells to NK cells stimulated through either cytokines or antigen receptor *ex vivo*. Strikingly, only NK cells stimulated through antigen receptor showed a strong correlation with the Nur77^{high} NK cells for both RNA-seq and ATAC-seq comparisons (**Fig. 3F** and **Supp. Fig. 2B**), as shown for the antigen-receptor regulated gene *Crtam* (**Fig. 3F**). Thus, our data suggest antigen receptor rather than cytokine signals drive the most dominant epigenetic and transcriptional changes in the NK cells that first respond to viral infection.

Antigen receptor signaling increases accessibility of regions bound by STAT4

Because antigen receptor signaling facilitates rapid epigenetic remodeling of NK cells *in vivo* and *in vitro*, we further characterized the genomic regions changing in the early antigen-experienced Nur77^{high} NK cells. In motif analysis, accessible regions were enriched for transcription factors known to be downstream of antigen receptor signaling, including BATF, Nr4a1, Egr, NFkB and NFAT (**Fig. 4A**). Since antigen-activated NK cells subsequently receive cytokine signaling (which peaks at day 2 PI), we hypothesized that

antigen receptor signaling may epigenetically alter genomic sites later bound by STAT transcription factors downstream of cytokine receptors. We compared differentially accessible regions to STAT1, STAT4 and STAT5 ChIP-seq datasets, and found an enrichment of regions that were bound by STAT4 and, to a lesser degree, STAT5 (**Fig. 4B**). Because the major cytokine driving STAT4 phosphorylation in NK cells is IL-12, we performed a STAT4 CUT&RUN in IL-12 stimulated NK cells with or without pre-stimulation with antigen receptor signaling, and observed a significant increase in STAT4 binding when antigen receptor was first ligated (**Fig. 4C**). Thus, early activating receptor signaling may epigenetically poise antigen-specific NK cells in preparation for subsequent binding of STAT4 when they later encounter proinflammatory cytokines.

Antigen receptor signaling synergizes with IL-12 signaling via epigenetic remodeling

Because our data suggests antigen receptor signaling facilitates STAT4 binding, we hypothesized that antigen receptor and IL-12 signals synergize to optimally prime NK cells. To directly test this, we analyzed NK cells that had been stimulated sequentially with antigen receptor plus IL-12 (or either antigen receptor or IL-12 alone) by RNA-seq (**Fig. 4D**. The majority of DE genes were synergistically upregulated or downregulated by the combination of antigen receptor plus IL-12 (**Fig. 4E**). In addition, we performed CUT&RUN for H3k4me3, a permissive histone mark for promoters (**Fig. 4F**). Histone modification by antigen receptor signaling contributed to the observed synergism, as DE genes synergistically upregulated also demonstrated a strong increase in H3K4me3 at

promoter sites after antigen receptor signaling, whereas DE genes synergistically downregulated showed a decrease in H3K4me3 signal (**Fig. 4F**).

Next, we assessed the biological processes most impacted by the observed synergistic regulation, and observed genes known to influence nutrient uptake and proliferation in NK cells, including *Myc*[19] and *Irf4*[20] (**Fig. 4G**). Antigen receptor enhancement of IL-12 signaling may also affect sensitivity to pro-proliferative signaling via IL-2 and IL-15, by boosting expression of *Stat5a* and the high-affinity IL-2 receptor *Il2ra*[21]. Altogether, our data suggests antigen receptor signaling synergizes with IL-12 signaling, in part by opening binding sites for STAT4 and in part by modulating permissive histone H3K4me3 levels at synergistically regulated genes.

Antagonistic regulation of key differentiation genes by antigen receptor versus IL-12 signaling

Although the majority of genes was synergistically regulated by antigen receptor signaling and IL-12, a substantial number of genes were regulated in an antagonistic manner (i.e. induced by one stimulus and repressed by the other) (**Fig. 4E**). Interestingly, antagonistically-regulated genes were linked to specific biological processes, including those involved in NK cell maturation and differentiation. In the absence of prior antigen receptor signaling, IL-12 upregulated expression of the maturation marker *Klrg1* and suppressed gene expression of *Cd27* and a negative regulator of NK cell maturation *Bach2*[22] (**Fig. 4H**). Thus, NK cells exposed to IL-12 alone demonstrate accelerated maturation, in contrast to those cells that first receive antigen receptor signaling.

The antagonistic regulation of key genes involved in maturation of NK cells suggests that antigen receptor signaling may oppose, while IL-12 promotes, the over-activation and/or terminal differentiation of NK cells. Although CD27 and KLRG1 were antagonistically regulated, CD11b (*Itgam*) expression was synergistically downregulated by sequential stimulation with antigen-receptor signaling and IL-12 (**Fig. 5A**). To assess effects on NK cell maturation, we cultured sequentially-stimulated NK cells overnight and analyzed NK cells using flow cytometry. Indeed, IL-12 alone reduced expression of CD27 and increased expression of KLRG1, while antigen receptor signaling alone showed the opposite effect, and neither demonstrated synergy in either direction when combined (**Fig. 5B**). In contrast, the maturation marker CD11b was synergistically downregulated by antigen receptor signaling and IL-12 (**Fig. 5B**).

The antagonistic regulation of CD27 and KLRG1 and synergistic regulation of CD11b were accompanied by corresponding epigenetic changes in the respective gene loci (**Fig. 5C**). For CD27, antigen receptor increased H3K4me3 at the *Cd27* promoter and increased accessibility of a region upstream of *Cd27*, thereby facilitating STAT4 binding. For CD11b, antigen-receptor signaling similarly increased binding of STAT4 to the promoter and two regions directly upstream and downstream of the gene. This could mean that STAT4 acts as an inducer of the *Cd27* but a repressor of the *Itgam* gene[23]. Flow cytometric analysis of NK cells stimulated sequentially or alone for maturation subset distribution revealed that only sequentially stimulated NK cells will specifically demonstrate enrichment of $CD27^{+}$ $CD11b^{-}$ NK cells, representing the least differentiated phenotype (**Fig. 5D**). These results together suggest that dual signals from antigen

receptor and cytokines protect NK cells from a differentiation fate involving improper accelerated maturation.

Antigen receptor signaling antagonizes IL-12 dependent terminal maturation

Previously, we and others have shown that less mature NK cells have an increased proliferative capacity during adaptive NK cell responses[10,24]. Because sequential stimulation with antigen receptor signaling and IL-12 increased the proportion of CD27$^+$ CD11b$^-$ NK cells, we sorted different subsets of NK cells and compared their expansion potential during MCMV infection. Indeed, sorted CD27$^+$ CD11b$^-$ NK cells showed the greatest expansion during MCMV infection, compared to CD27$^+$ CD11b$^+$ and CD27$^+$ CD11b$^-$ populations (**Fig. 5E**). Thus, retaining an immature phenotype, as observed in sequential stimulation, may contribute to the observed optimal expansion of the early antigen-experienced NK cells.

To test the antagonistic regulation of NK cell maturation during MCMV infection *in vivo*, we generated competitive WT:*Il12rb2*$^{-/-}$ chimeric mice and infected them with MCMV. *Il12rb2*$^{-/-}$ NK cells were previously described to expand poorly during the first week following MCMV infection[25]. However, this defect was not visible during the early days of infection with MCMV, where *Il12rb2*$^{-/-}$ NK cells were actually enriched compared to WT controls at day 2 PI (**Fig. 5F**). This enrichment coincided with *Il12rb2*$^{-/-}$ NK cells showing a more immature CD27$^+$ CD11b$^-$ and KLRG1$^-$ phenotype (**Fig. 5G**). Comparing the ratio of WT to *Il12rb2*$^{-/-}$ NK cells, Ly49H$^+$ and Ly49H$^-$ NK cell subsets similarly decreased on day 2 PI, but by day 4 PI the WT Ly49H$^+$ outgrew the Ly49H$^-$ NK cells (**Fig. 5H**). If antigen receptor signaling antagonized IL-12 driven terminal maturation, we would

expect antigen receptor expressing Ly49H$^+$ NK cells to be less mature than Ly49H$^-$ NK cells early during infection. Indeed, Ly49H$^+$ NK cells showed higher expression of CD27 and lower expression of KLRG1 than Ly49H$^-$ counterparts (**Fig. 5I**), suggesting that early antigen receptor signaling protects NK cells against IL-12 mediated, accelerated terminal maturation *in vivo*.

Antigen-receptor signaling alleviates IL-12 driven inhibition of proliferation

Because of the unexpected negative effect of IL-12 on NK cell expansion and maturation early during MCMV infection, we tested whether we can observe this effect in controlled experiments *in vitro*. WT and *Il12rb2*$^{-/-}$ NK cells were labeled with CellTrace Violet (CTV) stimulated with antigen-receptor (or unstimulated) followed by IL-12, and then cultured in IL-15 for 3 days (**Fig. 6A**). We observed that *Il12rb2*$^{-/-}$ NK cells outcompeted WT NK cells in the presence of IL-12, showing that the negative effect of IL-12 on NK cell expansion was recapitulated *in vitro* (**Fig. 6B**). This negative effect was partially rescued when NK cells were pre-stimulated through their antigen receptor. Furthermore, CTV dilution in WT NK cells was greatly reduced in NK cells stimulated with IL-12 alone, with antigen receptor pre-stimulation able to restore proliferation (**Fig. 6C**). The overall number of divisions attributable to antigen receptor signaling or lack thereof was similar, suggesting that the main parameter affected by sequential stimulation was the pool of cells in division rather than proliferation speed.

Antigen receptor signaling and IL-12 cooperate to sustain CDK6 expression

Cell cycle entry is tightly regulated by cyclin-dependent kinases, in particular CDK4 and CDK6[26]. In our RNA-seq analysis, CDK4 showed synergistic expression, whereas CDK6 appeared to be predominantly induced by antigen receptor signaling (**Fig. 6D**). However, CDK4 showed no difference in chromatin accessibility, H3K4me3 or STAT4 binding, whereas CDK6 showed multiple intergenic peaks that were not bound by STAT4 without prior antigen receptor signaling. To assess whether the immediate synergistic regulation of CDK4 or epigenetic regulation of CDK6 could explain differences in proliferation, we performed sequential stimulation of NK cells and stained for CDK4 and CDK6 after 24h (**Fig. 6E**). Although CDK4 did not show major differences in MFI or %, CDK6 was induced by IL-12 and a higher percentage of NK cells was positive for CDK6 after sequential stimulation with antigen-receptor signaling followed by IL-12. In agreement with this *in vitro* data, only CDK6 showed a substantial and IL-12 dependent difference between Ly49H$^+$ and Ly49H$^-$ NK cells from MCMV infected mice (**Fig. 6F**). Interestingly, the canonical proliferation marker Ki67 showed a contrary effect (**Supp. Fig. 3A**). IL-12 induced whereas antigen-receptor signaling repressed Mki67 expression at the mRNA level. *In vitro* sequential stimulation showed no difference between different conditions and Ki67 appeared, if anything, slightly downregulated compared in Ly49H$^+$ compared to Ly49H$^-$ NK cells *in vivo*.

Epigenetic Bim regulation via antigen receptor signaling suppresses apoptosis

Recently, it has been shown in human NK cells that antigen receptor signaling synergizes with IL-12 directly via mTOR signaling[27]. Our RNA-seq analysis suggested that this effect

may be supported by synergistic epigenetic regulation of both the *Mtor* and *Rps6* genes, and we could observe a moderate synergism for mTor *in vitro* (**Supp. Fig. 3B**).

Finally, we assessed cell death in NK cells receiving antigen receptor versus IL-12 versus sequential signals. The pro-apoptotic gene *Bim (Bcl2l11)* was antagonistically regulated by antigen receptor signaling and IL-12, with antigen receptor signaling suppressing and IL-12 upregulating expression (**Fig. 6G**). Epigenetically, antigen receptor signaling increased accessible regions upstream of the Bim (*Bcl2l11*) promoter, which only showed STAT4 binding after antigen receptor signaling (**Fig. 6G**). *In vitro*, sequential stimulation led to a specific downregulation of Bim and a decrease in the normalized Bim/Bcl2 ratio, which is crucial for the decision to undergo apoptosis[28] (**Fig. 6H**). Stimulation with IL-12 alone instead increased the Bim/Bcl2 ratio. Finally, Bim was selectively downregulated in Ly49H$^+$ over Ly49H$^-$ NK cells *in vivo* (**Fig. 6I**). Thus, regulation of Bim by external signals may help explain why IL-12 induces a short-lived effector cell fate. Thus, we conclude that antigen receptor signaling epigenetically reprograms NK cells to prevent terminal maturation mediated by cytokines alone, by enabling sustained CDK6 expression and downregulating apoptosis via Bim, and allowing for optimal clonal expansion of NK cells.

DISCUSSION

During systemic virus infections, inflammatory cytokines are thought to be among the first signals that immune cells encounter. Because we recently observed that tissue-resident NK cells form antigen-specific clusters as early as 24 hours following infection[10], we investigated the exact sequence of virus-induced signals received by NK cells. Here, we provide evidence that antigen-receptor signaling precedes cytokine signaling *in vivo*, and describe the downstream molecular events that subsequently unfold.

Although we confirmed that tissue-resident NK cells expand following MCMV exposure, this subset comprised only a small proportion of the antigen-experienced NK cells early after infection. Tissue-resident NK cells can both exist prior to infection[10], or attain residency following infection in tissues such as the salivary gland[11,29]. Fittingly, Nur77^{high} NK cells showed a phenotype known to be enriched in lymphoid organs and Nur77^{low} NK cells were phenotypically similar to circulating blood NK cells[30]. Thus, we propose that early antigen experienced NK cells are composed both by bona fide tissue resident and circulatory NK cells that are patrolling lymphoid organs at the time of antigen encounter.

Early antigen receptor signaling in NK cells during MCMV infection likely plays a crucial role for early viral clearance as previous studies suggested[31]. Moreover, it is attractive to speculate that antigen-specific NK cells could represent a key early orchestrator of the initial immune response by recruiting other immune cells rather than being recruited themselves. Among the genes immediately upregulated in early antigen experienced NK cells are CCL3, CCL4 and XCL1, which have previously been found to be released by CD8^{+} T cells to attract cDC1 and pDCs to form optimal niches for antigen

presentation during viral infection[32]. We and others have found NK-cDC1 crosstalk to be crucial for eliciting efficient immune responses[10,33-35] and $CD8^+$ T cells also express CCR5[36], the ligand for CCL3 and CCL4. Thus, antigen-specific NK cells may act as an early sentinel recruiting both innate and adaptive cells to elicit an optimal immune response[10].

The immediate epigenetic remodeling in antigen-experienced NK cells alters IL-12 signaling via STAT4 to promote the adaptive NK cell response via two potential mechanisms. Firstly, antigen receptor signaling can increase or decrease levels of H3K4me3 at promoters of STAT4-dependent genes, and the distribution of H3K4me3 has been shown to be crucial for memory T cell function[37]. In the future, we hope to better understand how antigen receptor signaling differentially methylates or demethylates H3K4 at different promoters, and how these processes are mediated[38]. Secondly, antigen receptor signaling modulates STAT4 signaling by increasing chromatin accessibility at otherwise closed genomic regions bound by STAT4. How these mechanisms shape the integration of other cytokine signals, including those of the common gamma chain family, remains to be determined. To this end, we have also observed an increase of accessibility of STAT5 binding sites in early antigen experienced NK cells. STAT5 is crucial for expansion of antiviral NK cells[21] and $CD8^+$ T cells[39] and has been shown to synergize with antigen-receptor signaling[40].

Our findings suggest that the synergy and antagonism of antigen receptor signaling and IL-12 may be a crucial mechanism influencing the fate decision of NK cells driving innate and adaptive states. Biologically, it makes sense that NK cells not harboring an antigen receptor are driven into a terminally mature effector fate incapable of

substantial proliferation. During MCMV infection, Ly49H$^-$ NK cells could optimally participate in innate functions (e.g. IFN-γ secretion) as bystanders, while not taking up space for the adaptive response of Ly49H$^+$ NK cells. Such a clonal competition mechanism has been previously proposed for T cell responses. Type I IFNs have been shown to suppress bystander T cells to ensure availability of niches for antigen-specific T cells to expand[41,42]. Because type I IFNs can signal through STAT4 (in addition to the canonical STAT1/STAT2/IRF9 complex), TCR signaling may similarly promote epigenetic remodeling in preparation for STAT4 binding. In support of this hypothesis, studies have found that TCR signaling decreases STAT1 while increasing STAT4 activity (via type I IFN), which was essential for clonal expansion[43,44]. Future studies will address how qualitative and quantitative differences in antigen receptor signaling shape innate and adaptive fates in different lymphocyte populations via epigenetic control of STAT binding.

Finally, how antigen receptor signaling affects integration of subsequent cytokine signaling is of crucial importance for the translation of immunotherapies, in particular adoptive cell therapy. Protocols for modification and expansion of therapeutic T cells rely on sequential stimulation with TCR signals along with cytokines[45], whereas NK cells used for adoptive therapy are expanded using cytokine cocktails or cytokine-expressing feeder cells[46-48]. The in-depth study of the precise genetic events following antigen receptor (via naturally expressed receptors or CARs) and cytokine signaling in NK cells will inform optimal targeted design of immune cells for adoptive cell therapy.

MATERIALS AND METHODS

Mice

All mice used in this study were housed and bred under specific-pathogen-free conditions with food and water in 12-h light–dark cycles at 72 °F with 30–70% humidity at Memorial Sloan Kettering Cancer Center and handled in accordance with the guidelines of the Institutional Animal Care and Use Committee. The following mouse strains were used in this study: C57BL/6 (CD45.2), C57BL/6 CD45.1 (CD45.1), C57BL/6 CD45.1×CD45.2, Il12rb2$^{-/-}$, Klra8$^{-/-}$ CD45.1xCD45.2 (Ly49H-deficient) and Ncr1-GFP and Nr4a1-GFP. Experiments were conducted using 8–10-week-old mice or 8–16 weeks post-transplant mixed bone-marrow chimeric mice and all experiments were conducted using age- and sex-matched mice in accordance with approved institutional protocols.

Virus

MCMV (Smith strain) was serially passaged through BALB/c hosts three times and then salivary gland viral stocks were prepared with a homogenizer for dissociating the salivary glands of infected mice 3 weeks after infection.

Mixed bone-marrow chimeras

Mixed bone-marrow chimeric (mBMC) mice were generated by lethally irradiating (950 cGy) C57BL/6 CD45.1×CD45.2 animals and reconstituting with a 1:1 mixture of bone-marrow cells from WT (CD45.1) and Il12rb2$^{-/-}$ (CD45.2) mice. Hosts were co-injected with anti-NK1.1 (PK136) to deplete any residual donor and host NK cells. Residual CD45.1^{+}CD45.2^{+} host NK cells were excluded from all analyses

Infections of Nr4a1-GFP mice and mixed bone marrow chimera

Chimerism in WT : IL12rb2$^{-/-}$ chimera was assessed by blood staining 1-2 weeks prior to the experiment. Nr4a1-GFP mice and bone marrow chimera were infected i.p. with 5 x 10^3 PFU of MCMV and analyzed at the respective time points using flow cytometry.

Isolation of mouse NK cells and flow cytometry

Spleens were dissociated with glass slides and filtered through a 100-µm cell strainer. Flow cytometry experiments were analyzed using a Cytek Aurora (Cytek Biosciences). Cell sorting was performed using a BD Aria II cytometers (BD Biosciences). Before cell sorting, NK cells were enriched by incubating whole splenocytes with the following antibodies at 10 µg/ml: CD3ε (Clone 17A2), CD4 (Clone GK1.5), CD8 (Clone 2.43), Ter119 (Clone TER-119), CD19 (Clone 1D3), Ly6G (Clone 1A8) (BioXCell). After washing, cells were incubated with goat anti-rat beads (QIAGEN, cat. no. 310107). For intracellular staining, cells were fixed and permeablizied using eBioscience Intracellular Fix & Perm Buffer Set (Thermo Fisher, cat. no. 88-8824-00).

Cell culture for *in vitro* experiments

NK cells were cultured in complete IMDM (10% FBS, 1× L-glutamine, 1× sodium pyruvate, 1× BME, 1× MEM-NAA and 25 mM HEPES). For cytokine stimulations, we used 50 ng/ml mouse IL-15 (Peprotech, cat. no. 210-15) and 20 ng/ml mouse IL-12 (R&D Systems, cat. no. 419-ML-050) depending on the experiment.

In vitro receptor and cytokine stimulation for sequencing

High-binding 96-well flat-bottom plates were coated with 100 µl per well of 20 µg/ml anti-NK1.1 (Clone PK136, BioLegend, cat. 108759) in PBS at 4 °C overnight. To prevent antigen-receptor signaling in negative controls, we used negative enrichment via magnetic beads and Ncr1-GFP mice. Splenic NK cells from Ncr1-GFP mice were purified using the NK Cell Isolation Kit (Miltenyi, cat. 130-115-818). Depending on the condition, NK cells were stimulated for 1-3h in 96 wells coated with anti-NK1.1 or in uncoated wells. After 1-3h, NK cells were either sorted for GFP positivity and directly used for sequencing or stimulated for 3h with IL-12. H3K4me3 CUT&RUN was performed after 1h of stimulation. RNA-seq was performed after 3h + 3h of stimulation. ATAC-seq was performed after 3h. STAT4 CUT&RUN was performed after 3h of aNK1.1 stimulation and 1h of IL-12 stimulation (aNK11 + IL-12), 3h of control stimulation in uncoated wells with full media and 1h of stimulation (IL-12 only) in control NK cells without stimulation.

CTV dilution and proliferation assay

Splenocytes from CD45.1/.1 (WT1), CD45.1/.2 (WT2) and IL12rb2$^{-/-}$ CD45.2/.2 (IL12rb2$^{-/-}$) were pooled and enriched using the NK Cell Isolation Kit (Miltenyi, Cat. 130-115-818). For CTV assays, cells were stained with CellTrace Violet (CTV) according to the manufacturer's instructions (Thermo Scientific, cat. C34557). NK cells were then stimulated in aNK1.1. coated plates and stimulated with cytokines according to the respective experiment. Sequential stimulation was performed as 3h of aNK1.1 and 3h of IL-12 stimulation before adding of IL-15 for overnight incubation. For CTV assays, NK cells were kept after sequential stimulation in aNK1.1 coated 96-well U-bottom plates overnight and then re-plated in 96-well U-Bottom plates without aNK1.1 coating for an additional 2 days.

Mouse single-cell RNA-sequencing and analysis

Splenic Ly49H$^+$ NK cells (CD3/TCRb/CD19−NK1.1$^+$CD49b$^+$Ly49H$^+$) from uninfected or MCMV-infected WT C57BL/6 mice were sorted as described and stained with barcoded antibodies (Total-Seq B, BioLegend). After hash-staining, NK cells were pooled and the single-cell RNA-seq from these pooled FACS-sorted cell suspensions was performed on a Chromium instrument (10x Genomics) following the user guide manual for 3′ v.3.1. In brief, FACS-sorted cells were washed once with PBS containing 1% bovine serum albumin (BSA) and resuspended in 1× PBS containing 1% BSA to a final concentration of 700–1,300 cells per µl. The viability of cells was above 80%, as confirmed with 0.2% (w/v) Trypan blue staining (Countess II). Cells were captured in droplets. Following reverse transcription and cell barcoding in droplets, emulsions were broken and cDNA-purified using Dynabeads MyOne SILANE (Thermo Fisher, cat. 37002D) followed by PCR amplification as per the manual instructions. Samples were multiplexed together on one lane of 10x Chromium (using Hash Tag Oligonucleotides (HTOs)). Final libraries were sequenced on Illumina NovaSeq6000 S4 platform (R1, 28 cycles; i7, 8 cycles; and R2, 90 cycles). The cell–gene count matrix was constructed using the 10x Cell Ranger (v7.1.0) pipeline based on mm10 2020-A reference. Viable cells were identified on the basis of library size and complexity, whereas cells with >20% of transcripts derived from mitochondria were excluded from further analysis. After mitochondrial and doublet cleanup, the raw count matrix was normalized by median library size normalization followed by log transformation. The Louvain algorithm with $k = 30$ was used to perform clustering and Euclidean distance was used as the metric to construct a nearest-neighbor. ‘Receptor signature’ was constructed from bulk RNA-seq data of naive NK cells

stimulated with anti-NK1.1 for 3 hours *in vitro*, while 'Cytokine signature' was obtained from GSEA mouse REACTOME gene set (R-MMU-1280215). All downstream analysis was done using scanpy (v1.9.0).

Bulk RNA sequencing. For data generated in this study, RNA was isolated from sorted cells and/or stimulated cells as described using PicoPure RNA Isolation Kit (ThermoFisher Scientific, cat. KIT0214). After RiboGreen quantification and quality control by Agilent BioAnalyzer. RNA was then amplified using SMART-Seq v.4 Ultra Low Input RNA kit (Clontech, cat. 63488). Subsequently, amplified complementary DNA was used to prepare libraries with KAPA HyperPrep Kit (Kapa Biosystems, cat. KK8504). Samples were barcoded and ran on NovaSeq6000 in a 100bp/100bp paired-end run.

Bulk ATAC sequencing. ATAC-seq was performed as described previously[49]. Briefly, sorted, stimulated cells were washed in cold PBS and lysed. The transposition reaction was incubated at 37 °C for 30 min. DNA was cleaned with the MinElute PCR Purification kit (QIAGEN, cat. 28004) and material was amplified for 5 cycles. After evaluation by real-time PCR, 8–11 additional PCR cycles were performed. The final product was cleaned by AMPure XP beads (Beckman Coulter catalog no. A63882) at a 1× ratio, and size selection was performed at a 0.5× ratio. Libraries were sequenced on a NovaSeq6000 in a 100 bp/100 bp paired-end run, using the NovaSeq6000 S2 or S4 Reagent kit (Illumina).

Histone and transcription factor CUT&RUN. For CUT&RUN, 100,000 and 500,000 sorted total NK cells were used for H3K4me3 and STAT4 CUT&RUN, respectively, and were treated as described above (see Method). For each target, anti-H3K4me3 (Epicypher, cat. 13-0041) or polyclonal anti-STAT4 antibodies (ThermoFisher, cat. 71-

4500) were used. Briefly, sorted cells were washed with PBS and resuspended in Antibody Buffer (1X eBioscience Perm/Wash Buffer, 1X Roche cOmplete EDTA-free Protease Inhibitor, 0.5 uM Spermidine, + 2uM EDTA in H_2O), and were incubated with control IgG, H3K4me3, or STAT4 antibodies at 1/100 dilution in Antibody Buffer in 96 well V-bottom plate at 4°C overnight. Upon antibody incubation, cells were washed twice with Buffer 1 (1X eBioscience Perm/Wash Buffer, 1X Roche cOmplete EDTA-free Protease Inhibitor, 0.5 uM Spermidine in H_2O) and resuspended in 50ul of Buffer 1 + 1X pA/G-MNase (Cell Signaling, cat. 57813) and incubated on ice for 1 hour and washed twice with Buffer 2 (0.05% w/v Saponin, 1X Roche cOmplete EDTA-free Protease Inhibitor, 0.5 uM Spermidine in 1X PBS) three times. After washing, Calcium Buffer (Buffer 2 + 2uM of $CaCl_2$) was used to resuspend the cells for 30 mins on ice to activate the pA/G-MNase reaction, and equal volume of 2X STOP Buffer (Buffer 2 + 20uM EDTA + 4uM EGTA) was added along with 1 pg of *Saccharomyces cerevisiae* spike-in DNA (Cell Signaling, cat. 29987). Samples were incubated for 15 mins at 37°C and DNA was isolated and purified using Qiagen MinElute Kit according to manufacturer's protocol and subjected to library amplification[50,51].

RNA-seq, ChIP-seq, CUT&RUN, and ATAC-seq data processing. Data processing methods for published RNA-seq, ChIP-seq, and ATAC-seq datasets have been previously described [Gabi NI, Moritz SciImmunol]. For RNA-seq dataset generated in this study, transcript quantification was based on the mm10 University of California, Santa Cruz (UCSC) Known Gene models and performed using the quasi-mapping-based mode of Salmon (v0.13.1) correcting for potential GC bias. Transcript was summarized to gene

level using tximport (v1.10.1). For CUT&RUN datasets found in this study, paired reads were trimmed for adaptors and removal of low-quality reads by using Trimmomatic (version 0.39) and aligned to the mm10 reference genome using Bowtie 2 (v2.4.1). Upon alignment, peaks were called using MACS2 (v2.2.7.1) with input samples as a control using narrow peak parameters with cutoff-analysis -p 1e-5 –keep-dup all -B –SPMR. For each sample group, irreproducible discovery rate (IDR) calculations were performed using scripts provided by the ENCODE project (IDR v2.0.4.2). For both CUT&RUN and ATAC-seq data, reproducible peaks showing an IDR value of 0.05 or less in each condition were retained, aggregated across the experiment and merged via union generate the final atlas, and annotated with the UCSC Known Gene model. Reads were mapped to the final atlas and counted with the summarizeOverlaps function from the GenomicAlignment package (v1.34.1).

Downstream analyses of bulk RNA-seq and ATAC-seq. For data generated in this study, differential analyses were executed with DESeq2 (v1.38.3) using UCSC Known Gene models as reference annotations. For RNA-seq or ATAC-seq, genes or peaks are considered differential if they showed p-adjusted value of < 0.05, adjusted for multiple hypothesis correction. Motif enrichment analysis was conducted using HOMER algorithm (HOMER v.4.10) using regions that showed differential accessibility ($p_{adj} < 0.05$ & $|log2FoldChange| > 0.5$) found between conditions with parameter '–size given –len 6,8,10,12,15 –mset vertebrates –mast' for de novo motif analysis. For correlation analyses, spearman coefficients were calculated using log_2FC modeled by DESeq2 when comparing between conditions on either shared differential features (genes or peaks) for each condition, or all shared features.

Visualization of RNA-seq, CUT&RUN and ATAC-seq. For peak-centered heatmaps and tracks, BAM files were converted to bigwig files using bamCoverage function and scaled based on sizeFactor modeled by DESeq2. Scaled bigwig files from each replicate per condition were then averaged using bigwigAverage function from deepTools (v3.5.4). All heatmaps from CUT&RUN and ATAC-seq experiments were plotted using EnrichedHeatmap (v1.28.1), while heatmaps from RNA-seq data were plotted using ComplexHeatmap (v2.14.0). All genomic tracks were either visualized by GViz (v1.42.1) or IGV (v2.9.4)

ACKNOWLEDGEMENTS

We thank members of the Sun lab, as well as the Single-Cell Analytics Innovation Lab (SAIL) at the Sloan Kettering Institute for technical support and experimental assistance, especially Dr. Ronan Chaligné. We acknowledge the use of the Integrated Genomics Operation Core, funded by the NCI Cancer Center Support Grant (CCSG, P30 CA08748) and the Marie-Josée and Henry R. Kravis Center for Molecular Oncology. S.G. is the recipient of a CRI / Donald J. Gogel Postdoctoral Fellowship (CRI Award #CRI3934). J.C.S. is supported by the Ludwig Center for Cancer Immunotherapy, the American Cancer Society, the Burroughs Wellcome Fund, and the NIH (AI100874, AI130043, and AI155558).

AUTHOR CONTRIBUTIONS

S.G., and J.C.S. designed the study. S.G., E.K.S., A.M.M, H.K., S.X.F. and M.O. performed experiments. E.K.S., H.K., and C.M.L. performed bioinformatics analyses. J.C.S provided critical resources and supervision for the study. S.G., E.K.S and J.C.S. wrote the manuscript.

DECLARATION OF INTERESTS

The authors declare no competing interests.

FIGURE LEGENDS

Figure 1: Early antigen-receptor signature in NK cells reacting to MCMV. A) UMAP projection of single-cell transcriptomes marked by different hashtags for uninfected NK cells and NK cells from days 1, 2, 3 or 4 PI. **B)** Louvain Clustering of scRNAseq analysis and analysis of hashtag proportions in each identified cluster. Dotted line indicates cluster 9. **C)** (top) Isolated Louvain clustering of single-cell transcriptomes from day 1 post infection. Dotted line indicates cluster 4. (bottom) Top ranked genes for cluster 4. **D)** Example genes downstream of antigen receptor signaling enriched in Cluster 4. **E)** Cytokine and antigen receptor score in scRNAseq separated according to day PI.

Figure 2: Early antigen experienced NK cells during MCMV infection. A) Nur77-GFP signal in uninfected mice and on day 1 following MCMV infection. **B)** Nur77-GFP mean fluorescence intensity (MFI) in splenic NK cells on days 1, 2 and 3 PI. Data was normalized to MFI in uninfected mice. **C)** Ratio of Nur77-GFP MFI in Ly49H^{+} and Ly49H^{-} NK cells in different organs on days 1, 2 and 3 PI or uninfected. **D)** MFI ratios of Nur77-GFP in Ly49H^{+} and Ly49H^{-} NK cells early during infection and in different organs on day 1 PI. **E)** Phenotypic analysis of Ly49H^{+} Nur77-GFP^{high} and Ly49H^{+} Nur77-GFP^{low} NK cells at day 1 PI. **F)** Quantification of NK cell maturation states in Ly49H^{+} Nur77-GFP^{high} and Ly49H^{+} Nur77-GFP^{low} NK cells. **G)** Co-transfer of congenically marked Ly49H^{+} Nur77-GFP^{high} and Ly49H^{+} Nur77-GFP^{low} NK cells into infection matched Ly49H$^{-/-}$ mice.

Data are pooled from two individual experiments. Significances are calculated as paired T-test. **** $p < 0.0001$, *** $p < 0.001$, ** $p < 0.01$, * $p < 0.05$.

Figure 3: Transcriptomic and epigenetic analysis of early antigen-experienced NK cells. A) Sort of Ly49H$^+$ Nur77^{high}, Ly49H$^+$ Nur77^{low} and Ly49H$^-$ (Ly49D$^+$, not gated for Nur77) NK cells on day 1 PI. **B)** PCA plots of RNAseq and ATACseq from Ly49H$^+$ Nur77^{high}, Ly49H$^+$ Nur77^{low} and Ly49H$^-$ NK cells on day 1 PI. **C)** Heatmap of RNAseq of Ly49H$^+$ Nur77^{high}, Ly49H$^+$ Nur77^{low} and Ly49H$^-$ NK cells. **D)** Heatmap of ATACseq of Ly49H$^+$ Nur77^{high}, Ly49H$^+$ Nur77^{low} and Ly49H$^-$ NK cells. **E)** Peak type analysis of DA peaks in ATACseq. Comparison of Ly49H$^+$ Nur77^{high} and Ly49H$^+$ Nur77^{low} NK cells (left) and Ly49H$^+$ Nur77^{high} and Ly49H$^-$ NK cells (right). **F)** Spearman correlations of early antigen experienced NK cells with *in vitro* stimulated NK cells using RNAseq (Top) or ATACseq (Bottom). **G)** Example DA regions in early antigen experienced NK cells and antigen-receptor stimulated NK cells *in vitro*.

Figure 4: Synergism and antagonism of antigen receptor versus IL-12 signaling. A) Motif analysis of transcription factor motifs in DA regions of early antigen experienced NK cells. **B)** Comparison of accessibility of STAT1, STAT4 and STAT5 binding peaks as assessed with ChIPseq. **C)** Heatmap of STAT4 CUT&RUN in unstimulated, IL-12 stimulated or aNK1.1 + IL-12 sequentially stimulated NK cells. **D)** PCA of RNA-seq analysis of unstimulated, aNK1.1 stimulated, IL-12 stimulated or aNK1.1 + IL-12 sequentially stimulated NK cells. **E)** z-scores and heatmap of RNA-seq analysis. Grouping into antagonistic and synergistic genes. **F)** CUT&RUN for H3K4me3 in unstimulated and aNK1.1 stimulated NK cells. **G)** Ranks of synergistic upregulated genes. **H)** Volcano plots of RNA-seq analysis. Selected antagonistic genes were highlighted.

Figure 5: Antagonistic regulation of NK cell maturation driven by antigen receptor versus IL-12 signaling. A) Normalized reads of genes encoding for maturation markers

in RNAseq analysis. **B)** MFI of maturation markers in NK cells sequentially stimulated with aNK1.1 and IL-12 and cultured overnight in IL-15. **C)** H3K4me3 CUT&RUN, DA regions in ATACseq and STAT4 binding measured with CUT&RUN at genes encoding for maturation markers. **D)** Frequency of NK cells with distinct maturation states in overnight stimulated NK cells from B). **E)** Co-transfer of NK cells with different maturation states into Ly49H$^{-/-}$ NK cells and comparison of expansion at day 7 PI with MCMV. **F)** Expansion of NK cells in competitive WT : IL12rb2$^{-/-}$ chimera on day 2 and 4 PI with MCMV. **G)** Comparison of maturation markers in WT and IL12rb2$^{-/-}$ NK cells on day 2 PI. **H)** Comparison of relative expansion of Ly49H^{+} and Ly49H^{-} (Ly49D^{+}) NK cells in competitive WT : IL12rb2$^{-/-}$ chimera during MCMV infection. **I)** Expression of maturation markers in Ly49H^{+} and Ly49H^{-} (Ly49D^{+}) NK cells during MCMV infection.

Data in 5B) and 5D) are pooled from two independent experiments. Data in 5E is representative of two individual similar experiments. Data in 5F) – 5I) is pooled from 2-4 individual experiments. Significances are calculated using paired T-test. **** $p < 0.0001$, *** $p < 0.001$, ** $p < 0.01$, * $p < 0.05$.

Figure 6: Antagonistic regulation of NK cell proliferation and apoptosis by antigen receptor versus IL-12 signaling. A) Experimental setup: Sequential stimulation of WT and IL12rb2$^{-/-}$ NK cells with antigen-receptor signaling and IL-12, followed by expansion with IL-15. **B)** (left) Relative abundance of WT and IL12rb2$^{-/-}$ NK cells in representative flow cytometry plots. (right) Quantification of WT/IL12rb2$^{-/-}$ count ratio in different conditions. **C)** (left) Representative histograms showing CTV dilution. (right) quantification of divided WT NK cells (%), CTV MFI (all WT NK cells) and CTV MFI (divided NK cells). **D)** Normalized Reads of *Cdk4* and *Cdk6* in sequential stimulation and ATAC and

CUT&RUN peaks (H3K4me3 and STAT4) at *Cdk4* and *Cdk6* gene loci during stimulation. **E)** MFI ratio and % of CDK4 and CDK6 in sequentially stimulated NK cells 24h post stimulation. **F)** Normalized ratio of CDK4 and CDK6 MFI in competitive WT : IL12rb2$^{-/-}$ chimera in Ly49H^{+} and Ly49H^{-} (Ly49D^{+}) NK cells during MCMV infection. **G)** Normalized Reads of *Bcl2l11* in sequential stimulation and ATAC and CUT&RUN peaks (H3K4me3 and STAT4) at the *Bcl2l11* gene locus during stimulation. **H)** (left) MFI ratio of Bim in sequentially stimulated NK cells 24h post stimulation and (right) Bim/Bcl2 ratio. **I)** Normalized ratio of Bim MFI in competitive WT : IL12rb2$^{-/-}$ chimera in Ly49H^{+} and Ly49H^{-} (Ly49D^{+}) NK cells during MCMV infection.

Data in 6B) and 6C) are representative of two independent and 4 similar experiments. Data in 6E), 6F), 6H) and 6I) were pooled from two independent experiments. Significances are calculated using paired T-test. **** $p < 0.0001$, *** $p < 0.001$, ** $p < 0.01$, * $p < 0.05$.

Supp. Fig. 1: Ranking of genes in different Louvain clusters on day 1 post infection.

Supp. Fig. 2: **A)** Comparison of DA regions and peak type in Ly49H^{+} Nur77^{low} and Ly49H^{-} NK cells. **B)** Scatter plots showing correlation of RNA-seq and ATAC-seq data from Nur77^{high} vs. Nur77^{low} Ly49H^{+} NK cells with *in vitro* stimulated NK cells. *R* = Spearman correlation coefficient.

Supp. Fig. 3: **A)** (left) Normalized reads of *Mki67*. (middle) MFI ratios of Ki67 (WT/IL12rb2$^{-/-}$) after sequential stimulation *in vitro*. (right) MFI ratios of Ki67 (WT/IL12rb2$^{-/-}$) in Ly49H^{+} and Ly49H^{-} (Ly49D^{+}) NK cells during MCMV infection. **B)** (left) Normalized reads of *Mtor* and *Rps6*. (middle) MFI ratios of mTor and pS6 (WT/IL12rb2$^{-/-}$) after

sequential stimulation *in vitro*. (right) MFI ratios of mTor and pS6 (WT/IL12rb2$^{-/-}$) in Ly49H^{+} and Ly49H^{-} (Ly49D^{+}) NK cells during MCMV infection.

REFERENCES

1 Sun, J. C., Beilke, J. N. & Lanier, L. L. Adaptive immune features of natural killer cells. *Nature* **457**, 557-561, doi:10.1038/nature07665 (2009).

2 Gumá, M. n., Angulo, A., Vilches, C., Gómez-Lozano, N., Malats, N. r. & López-Botet, M. Imprint of human cytomegalovirus infection on the NK cell receptor repertoire. *Blood* **104**, 3664-3671, doi:10.1182/blood-2004-05-2058 (2004).

3 Björkström, N. K., Lindgren, T., Stoltz, M., Fauriat, C., Braun, M., Evander, M., Michaëlsson, J., Malmberg, K.-J., Klingström, J., Ahlm, C. & Ljunggren, H.-G. Rapid expansion and long-term persistence of elevated NK cell numbers in humans infected with hantavirus. *The Journal of experimental medicine* **208**, 13-21, doi:10.1084/jem.20100762 (2011).

4 Arase, H., Mocarski, E. S., Campbell, A. E., Hill, A. B. & Lanier, L. L. Direct recognition of cytomegalovirus by activating and inhibitory NK cell receptors. *Science* **296**, 1323-1326, doi:10.1126/science.1070884 (2002).

5 Smith, H. R. C., Heusel, J. W., Mehta, I. K., Kim, S., Dorner, B. G., Naidenko, O. V., Iizuka, K., Furukawa, H., Beckman, D. L., Pingel, J. T., Scalzo, A. A., Fremont, D. H. & Yokoyama, W. M. Recognition of a virus-encoded ligand by a natural killer cell activation receptor. *Proceedings of the National Academy of Sciences* **99**, 8826, doi:10.1073/pnas.092258599 (2002).

6 Hammer, Q., Rückert, T., Borst, E. M., Dunst, J., Haubner, A., Durek, P., Heinrich, F., Gasparoni, G., Babic, M., Tomic, A., Pietra, G., Nienen, M., Blau, I. W., Hofmann, J., Na, I.-K., Prinz, I., Koenecke, C., Hemmati, P., Babel, N., Arnold, R., Walter, J., Thurley, K., Mashreghi, M.-F., Messerle, M. & Romagnani, C. Peptide-specific recognition of human cytomegalovirus strains controls adaptive natural killer cells. *Nature Immunology* **19**, 453-463, doi:10.1038/s41590-018-0082-6 (2018).

7 Salazar-Mather, T. P., Orange, J. S. & Biron, C. A. Early murine cytomegalovirus (MCMV) infection induces liver natural killer (NK) cell inflammation and protection

through macrophage inflammatory protein 1alpha (MIP-1alpha)-dependent pathways. *J Exp Med* **187**, 1-14, doi:10.1084/jem.187.1.1 (1998).

8 Martín-Fontecha, A., Thomsen, L. L., Brett, S., Gerard, C., Lipp, M., Lanzavecchia, A. & Sallusto, F. Induced recruitment of NK cells to lymph nodes provides IFN-γ for TH1 priming. *Nature Immunology* **5**, 1260-1265, doi:10.1038/ni1138 (2004).

9 Dogra, P., Rancan, C., Ma, W., Toth, M., Senda, T., Carpenter, D. J., Kubota, M., Matsumoto, R., Thapa, P. & Szabo, P. A. Tissue determinants of human NK cell development, function, and residence. *Cell* **180**, 749-763. e713 (2020).

10 Flommersfeld, S., Böttcher, J. P., Ersching, J., Flossdorf, M., Meiser, P., Pachmayr, L. O., Leube, J., Hensel, I., Jarosch, S., Zhang, Q., Chaudhry, M. Z., Andrae, I., Schiemann, M., Busch, D. H., Cicin-Sain, L., Sun, J. C., Gasteiger, G., Victora, G. D., Höfer, T., Buchholz, V. R. & Grassmann, S. Fate mapping of single NK cells identifies a type 1 innate lymphoid-like lineage that bridges innate and adaptive recognition of viral infection. *Immunity* **54**, 2288-2304.e2287, doi:10.1016/j.immuni.2021.08.002 (2021).

11 Schuster, I. S., Sng, X. Y. X., Lau, C. M., Powell, D. R., Weizman, O. E., Fleming, P., Neate, G. E. G., Voigt, V., Sheppard, S., Maraskovsky, A. I., Daly, S., Koyama, M., Hill, G. R., Turner, S. J., O'Sullivan, T. E., Sun, J. C., Andoniou, C. E. & Degli-Esposti, M. A. Infection induces tissue-resident memory NK cells that safeguard tissue health. *Immunity* **56**, 531-546.e536, doi:10.1016/j.immuni.2023.01.016 (2023).

12 Liu, Z.-G., Smith, S. W., McLaughlin, K. A., Schwartz, L. M. & Osborne, B. A. Apoptotic signals delivered through the T-cell receptor of a T-cell hybrid require the immediate–early gene nur77. *Nature* **367**, 281-284 (1994).

13 McNeil, L. K., Starr, T. K. & Hogquist, K. A. A requirement for sustained ERK signaling during thymocyte positive selection in vivo. *Proceedings of the National Academy of Sciences* **102**, 13574-13579, doi:doi:10.1073/pnas.0505110102 (2005).

14 Safford, M., Collins, S., Lutz, M. A., Allen, A., Huang, C.-T., Kowalski, J., Blackford, A., Horton, M. R., Drake, C., Schwartz, R. H. & Powell, J. D. Egr-2 and

Egr-3 are negative regulators of T cell activation. *Nature Immunology* **6**, 472-480, doi:10.1038/ni1193 (2005).

15 Moran, A. E., Holzapfel, K. L., Xing, Y., Cunningham, N. R., Maltzman, J. S., Punt, J. & Hogquist, K. A. T cell receptor signal strength in Treg and iNKT cell development demonstrated by a novel fluorescent reporter mouse. *Journal of Experimental Medicine* **208**, 1279-1289 (2011).

16 Hsu, K. M., Pratt, J. R., Akers, W. J., Achilefu, S. I. & Yokoyama, W. M. Murine cytomegalovirus displays selective infection of cells within hours after systemic administration. *J Gen Virol* **90**, 33-43, doi:10.1099/vir.0.006668-0 (2009).

17 Mason, L. H., Anderson, S. K., Yokoyama, W. M., Smith, H. R. C., Winkler-Pickett, R. & Ortaldo, J. R. The Ly-49D Receptor Activates Murine Natural Killer Cells. *Journal of Experimental Medicine* **184**, 2119-2128, doi:10.1084/jem.184.6.2119 (1996).

18 Wiedemann, G. M., Santosa, E. K., Grassmann, S., Sheppard, S., Le Luduec, J.-B., Adams, N. M., Dang, C., Hsu, K. C., Sun, J. C. & Lau, C. M. Deconvoluting global cytokine signaling networks in natural killer cells. *Nature Immunology* **22**, 627-638, doi:10.1038/s41590-021-00909-1 (2021).

19 Dong, H., Adams, N. M., Xu, Y., Cao, J., Allan, D. S. J., Carlyle, J. R., Chen, X., Sun, J. C. & Glimcher, L. H. The IRE1 endoplasmic reticulum stress sensor activates natural killer cell immunity in part by regulating c-Myc. *Nat Immunol* **20**, 865-878, doi:10.1038/s41590-019-0388-z (2019).

20 Santosa, E. K., Kim, H., Rückert, T., Le Luduec, J.-B., Abbasi, A. J., Wingert, C. K., Peters, L., Frost, J. N., Hsu, K. C., Romagnani, C. & Sun, J. C. Control of nutrient uptake by IRF4 orchestrates innate immune memory. *Nature Immunology* **24**, 1685-1697, doi:10.1038/s41590-023-01620-z (2023).

21 Wiedemann, G. M., Grassmann, S., Lau, C. M., Rapp, M., Villarino, A. V., Friedrich, C., Gasteiger, G., O'Shea, J. J. & Sun, J. C. Divergent Role for STAT5 in the Adaptive Responses of Natural Killer Cells. *Cell Rep* **33**, 108498, doi:10.1016/j.celrep.2020.108498 (2020).

22 Li, S., Bern, M. D., Miao, B., Fan, C., Xing, X., Inoue, T., Piersma, S. J., Wang, T., Colonna, M., Kurosaki, T. & Yokoyama, W. M. The transcription factor Bach2

negatively regulates murine natural killer cell maturation and function. *eLife* **11**, e77294, doi:10.7554/eLife.77294 (2022).

23 Gonzales-van Horn, S. R., Estrada, L. D., van Oers, N. S. & Farrar, J. D. STAT4-mediated transcriptional repression of the IL5 gene in human memory Th2 cells. *Eur J Immunol* **46**, 1504-1510, doi:10.1002/eji.201546050 (2016).

24 Kamimura, Y. & Lanier, L. L. Homeostatic control of memory cell progenitors in the natural killer cell lineage. *Cell Rep* **10**, 280-291, doi:10.1016/j.celrep.2014.12.025 (2015).

25 Sun, J. C., Madera, S., Bezman, N. A., Beilke, J. N., Kaplan, M. H. & Lanier, L. L. Proinflammatory cytokine signaling required for the generation of natural killer cell memory. *J Exp Med* **209**, 947-954, doi:10.1084/jem.20111760 (2012).

26 Fassl, A., Geng, Y. & Sicinski, P. CDK4 and CDK6 kinases: From basic science to cancer therapy. *Science* **375**, eabc1495, doi:doi:10.1126/science.abc1495 (2022).

27 Shemesh, A., Pickering, H., Roybal, K. T. & Lanier, L. L. Differential IL-12 signaling induces human natural killer cell activating receptor-mediated ligand-specific expansion. *J Exp Med* **219**, doi:10.1084/jem.20212434 (2022).

28 Wojciechowski, S., Tripathi, P., Bourdeau, T., Acero, L., Grimes, H. L., Katz, J. D., Finkelman, F. D. & Hildeman, D. A. Bim/Bcl-2 balance is critical for maintaining naive and memory T cell homeostasis. *J Exp Med* **204**, 1665-1675, doi:10.1084/jem.20070618 (2007).

29 Grégoire, C., Chasson, L., Luci, C., Tomasello, E., Geissmann, F., Vivier, E. & Walzer, T. The trafficking of natural killer cells. *Immunol Rev* **220**, 169-182, doi:10.1111/j.1600-065X.2007.00563.x (2007).

30 Chiossone, L., Chaix, J., Fuseri, N., Roth, C., Vivier, E. & Walzer, T. Maturation of mouse NK cells is a 4-stage developmental program. *Blood* **113**, 5488-5496, doi:10.1182/blood-2008-10-187179 (2009).

31 Brown, M. G., Dokun, A. O., Heusel, J. W., Smith, H. R. C., Beckman, D. L., Blattenberger, E. A., Dubbelde, C. E., Stone, L. R., Scalzo, A. A. & Yokoyama, W. M. Vital Involvement of a Natural Killer Cell Activation Receptor in Resistance

to Viral Infection. *Science* **292**, 934-937, doi:doi:10.1126/science.1060042 (2001).

32 Brewitz, A., Eickhoff, S., Dähling, S., Quast, T., Bedoui, S., Kroczek, R. A., Kurts, C., Garbi, N., Barchet, W., Iannacone, M., Klauschen, F., Kolanus, W., Kaisho, T., Colonna, M., Germain, R. N. & Kastenmüller, W. CD8(+) T Cells Orchestrate pDC-XCR1(+) Dendritic Cell Spatial and Functional Cooperativity to Optimize Priming. *Immunity* **46**, 205-219, doi:10.1016/j.immuni.2017.01.003 (2017).

33 Ghilas, S., Ambrosini, M., Cancel, J.-C., Brousse, C., Massé, M., Lelouard, H., Dalod, M. & Crozat, K. Natural killer cells and dendritic epidermal γδ T cells orchestrate type 1 conventional DC spatiotemporal repositioning toward CD8+ T cells. *iScience* **24**, 103059, doi:https://doi.org/10.1016/j.isci.2021.103059 (2021).

34 Bottcher, J. P., Bonavita, E., Chakravarty, P., Blees, H., Cabeza-Cabrerizo, M., Sammicheli, S., Rogers, N. C., Sahai, E., Zelenay, S. & Reis e Sousa, C. NK Cells Stimulate Recruitment of cDC1 into the Tumor Microenvironment Promoting Cancer Immune Control. *Cell* **172**, 1022-1037.e1014, doi:10.1016/j.cell.2018.01.004 (2018).

35 Smyth, M. J., Crowe, N. Y. & Godfrey, D. I. NK cells and NKT cells collaborate in host protection from methylcholanthrene-induced fibrosarcoma. *Int Immunol* **13**, 459-463, doi:10.1093/intimm/13.4.459 (2001).

36 Kohlmeier, J. E., Miller, S. C., Smith, J., Lu, B., Gerard, C., Cookenham, T., Roberts, A. D. & Woodland, D. L. The chemokine receptor CCR5 plays a key role in the early memory CD8+ T cell response to respiratory virus infections. *Immunity* **29**, 101-113, doi:10.1016/j.immuni.2008.05.011 (2008).

37 Araki, Y., Wang, Z., Zang, C., Wood, W. H., 3rd, Schones, D., Cui, K., Roh, T. Y., Lhotsky, B., Wersto, R. P., Peng, W., Becker, K. G., Zhao, K. & Weng, N. P. Genome-wide analysis of histone methylation reveals chromatin state-based regulation of gene transcription and function of memory CD8+ T cells. *Immunity* **30**, 912-925, doi:10.1016/j.immuni.2009.05.006 (2009).

38 Hyun, K., Jeon, J., Park, K. & Kim, J. Writing, erasing and reading histone lysine methylations. *Experimental & Molecular Medicine* **49**, e324-e324, doi:10.1038/emm.2017.11 (2017).

39 Tripathi, P., Kurtulus, S., Wojciechowski, S., Sholl, A., Hoebe, K., Morris, S. C., Finkelman, F. D., Grimes, H. L. & Hildeman, D. A. STAT5 Is Critical To Maintain Effector CD8+ T Cell Responses. *The Journal of Immunology* **185**, 2116-2124, doi:10.4049/jimmunol.1000842 (2010).

40 Kelly, J. A., Spolski, R., Kovanen, P. E., Suzuki, T., Bollenbacher, J., Pise-Masison, C. A., Radonovich, M. F., Lee, S., Jenkins, N. A., Copeland, N. G., Morse, H. C., 3rd & Leonard, W. J. Stat5 synergizes with T cell receptor/antigen stimulation in the development of lymphoblastic lymphoma. *J Exp Med* **198**, 79-89, doi:10.1084/jem.20021548 (2003).

41 Dondi, E., Rogge, L., Lutfalla, G., Uzé, G. & Pellegrini, S. Down-Modulation of Responses to Type I IFN Upon T Cell Activation1. *The Journal of Immunology* **170**, 749-756, doi:10.4049/jimmunol.170.2.749 (2003).

42 Crouse, J., Kalinke, U. & Oxenius, A. Regulation of antiviral T cell responses by type I interferons. *Nature Reviews Immunology* **15**, 231-242, doi:10.1038/nri3806 (2015).

43 Gil, M. P., Ploquin, M. J., Watford, W. T., Lee, S. H., Kim, K., Wang, X., Kanno, Y., O'Shea, J. J. & Biron, C. A. Regulating type 1 IFN effects in CD8 T cells during viral infections: changing STAT4 and STAT1 expression for function. *Blood* **120**, 3718-3728, doi:10.1182/blood-2012-05-428672 (2012).

44 Gil, M. P., Salomon, R., Louten, J. & Biron, C. A. Modulation of STAT1 protein levels: a mechanism shaping CD8 T-cell responses in vivo. *Blood* **107**, 987-993, doi:10.1182/blood-2005-07-2834 (2006).

45 Stock, S., Schmitt, M. & Sellner, L. Optimizing Manufacturing Protocols of Chimeric Antigen Receptor T Cells for Improved Anticancer Immunotherapy. *Int J Mol Sci* **20**, doi:10.3390/ijms20246223 (2019).

46 Zhang, L., Meng, Y., Feng, X. & Han, Z. CAR-NK cells for cancer immunotherapy: from bench to bedside. *Biomarker Research* **10**, 12, doi:10.1186/s40364-022-00364-6 (2022).

47 Portillo, A. L., Hogg, R., Poznanski, S. M., Rojas, E. A., Cashell, N. J., Hammill, J. A., Chew, M. V., Shenouda, M. M., Ritchie, T. M., Cao, Q. T., Hirota, J. A., Dhesy-Thind, S., Bramson, J. L. & Ashkar, A. A. Expanded human NK cells armed with CAR uncouple potent anti-tumor activity from off-tumor toxicity against solid tumors. *iScience* **24**, 102619, doi:https://doi.org/10.1016/j.isci.2021.102619 (2021).

48 Liu, E., Marin, D., Banerjee, P., Macapinlac, H. A., Thompson, P., Basar, R., Nassif Kerbauy, L., Overman, B., Thall, P., Kaplan, M., Nandivada, V., Kaur, I., Nunez Cortes, A., Cao, K., Daher, M., Hosing, C., Cohen, E. N., Kebriaei, P., Mehta, R., Neelapu, S., Nieto, Y., Wang, M., Wierda, W., Keating, M., Champlin, R., Shpall, E. J. & Rezvani, K. Use of CAR-Transduced Natural Killer Cells in CD19-Positive Lymphoid Tumors. *N Engl J Med* **382**, 545-553, doi:10.1056/NEJMoa1910607 (2020).

49 Buenrostro, J. D., Giresi, P. G., Zaba, L. C., Chang, H. Y. & Greenleaf, W. J. Transposition of native chromatin for fast and sensitive epigenomic profiling of open chromatin, DNA-binding proteins and nucleosome position. *Nat Methods* **10**, 1213-1218, doi:10.1038/nmeth.2688 (2013).

50 Santosa, E. K., Lau, C. M., Sahin, M., Leslie, C. S. & Sun, J. C. 3D Chromatin Dynamics during Innate and Adaptive Immune Memory Acquisition. *bioRxiv*, 2023.2001.2016.524322, doi:10.1101/2023.01.16.524322 (2023).

51 Kim, H., Abbasi, A., Sharrock, J., Santosa, E. K., Sheppard, S., Lau, C. M., Edelson, B. T. & Sun, J. C. Cutting Edge: STAT4 Promotes Bhlhe40 Induction to Drive Protective IFN-γ from NK Cells during Viral Infection. *J Immunol*, doi:10.4049/jimmunol.2300402 (2023).

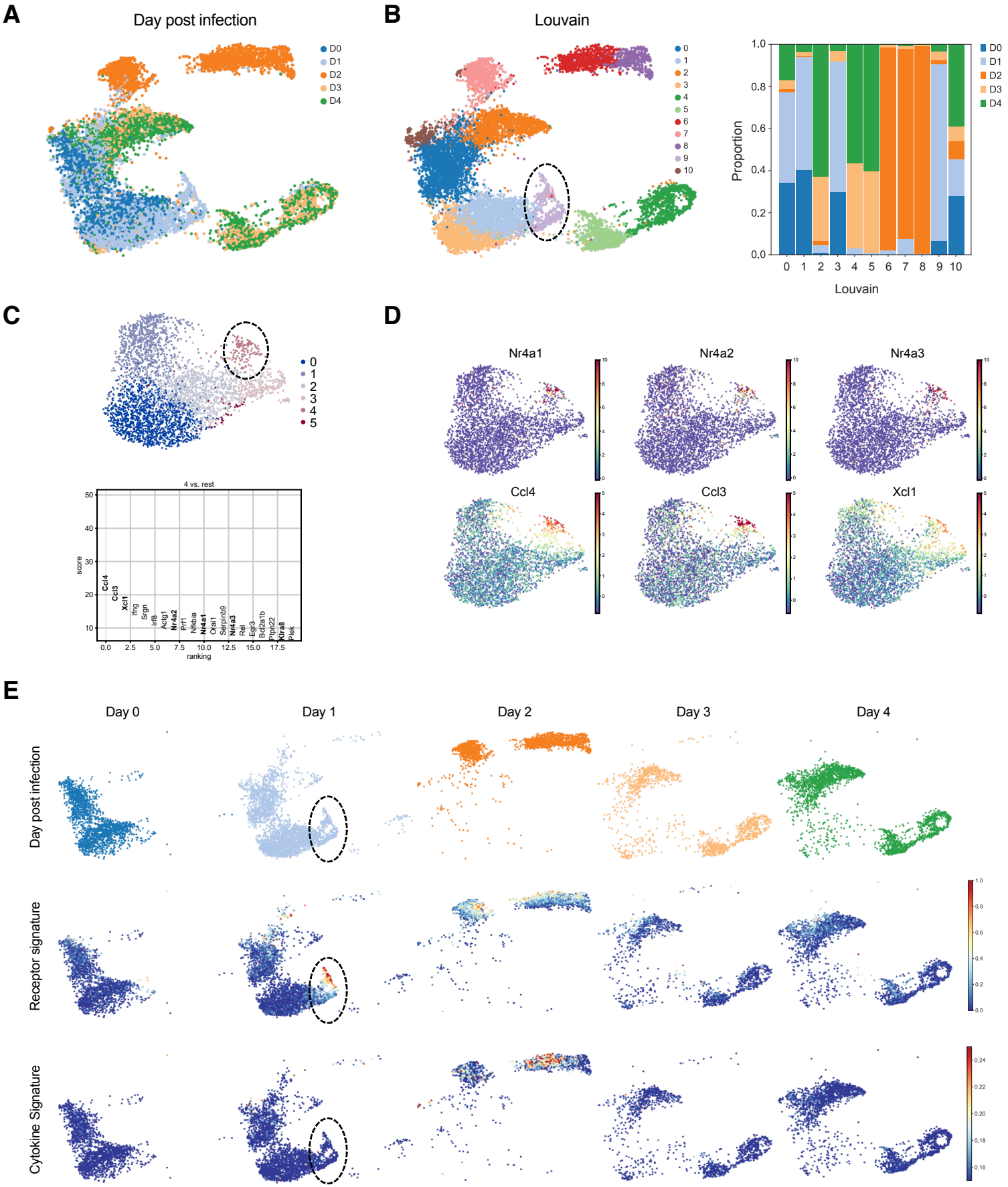
A
Day post infection
D0
D1
D2
D3
D4
B
Louvain
0
1
2
3
4
5
6
7
8
9
10
Proportion
Louvain
C
4 vs. rest
score
ranking
Ccl4
Ccl3
Xcl1
Ifng
Srgn
Irf8
Actg1
Nr4a2
Prf1
Nfkbia
Nr4a1
Orai1
Serpinb9
Nr4a3
Rel
Egr3
Bcl2a1b
Ptpn22
Klra8
Plek
D
Nr4a1
Nr4a2
Nr4a3
Ccl4
Ccl3
Xcl1
E
Day 0
Day 1
Day 2
Day 3
Day 4
Day post infection
Receptor signature
Cytokine Signature

Figure 1

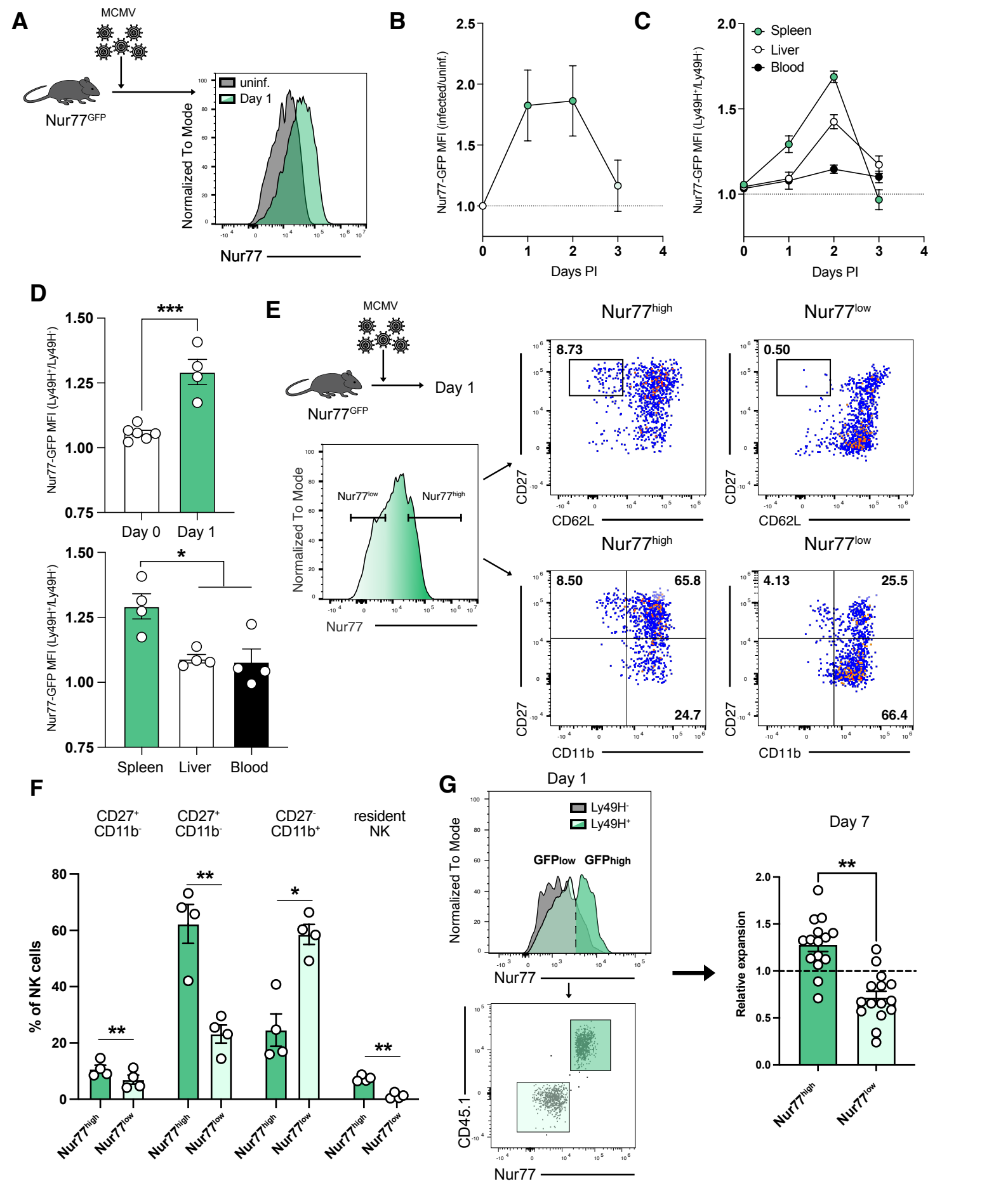
A
MCMV
Nur77GFP
uninf.
Day 1
Normalized To Mode
Nur77
B
Nur77-GFP MFI (infected/uninf.)
Days PI
C
Spleen
Liver
Blood
Nur77-GFP MFI (Ly49H+/Ly49H-)
Days PI
D
Nur77-GFP MFI (Ly49H+/Ly49H-)
Day 0
Day 1
Spleen
Liver
Blood
E
MCMV
Nur77GFP
Day 1
Nur77low
Nur77high
Normalized To Mode
Nur77
Nur77high
Nur77low
8.73
0.50
CD27
CD62L
8.50
65.8
24.7
4.13
25.5
66.4
CD11b
F
CD27+ CD11b-
CD27+ CD11b-
CD27- CD11b+
resident NK
% of NK cells
Nur77high
Nur77low
G
Day 1
Ly49H-
Ly49H+
GFPlow
GFPhigh
Normalized To Mode
Nur77
CD45.1
Day 7
Relative expansion
Nur77high
Nur77low

Figure 2

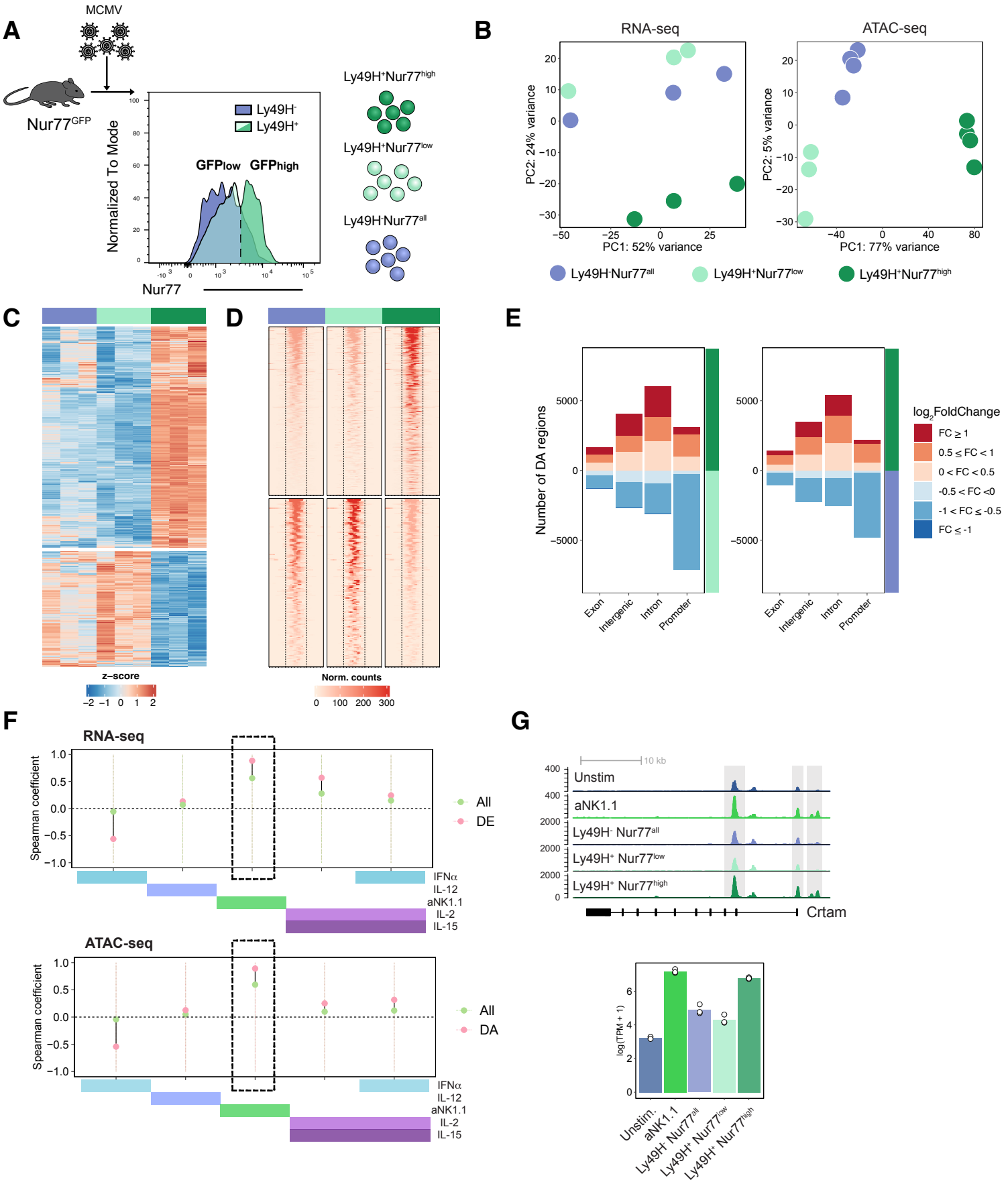
A
MCMV
Nur77GFP
Ly49H-
Ly49H+
GFPlow GFPhigh
Normalized To Mode
Nur77
Ly49H+Nur77high
Ly49H+Nur77low
Ly49H-Nur77all
B
RNA-seq
ATAC-seq
PC2: 24% variance
PC1: 52% variance
PC2: 5% variance
PC1: 77% variance
Ly49H-Nur77all
Ly49H+Nur77low
Ly49H+Nur77high
C
z-score
D
Norm. counts
E
Number of DA regions
Exon
Intergenic
Intron
Promoter
log2FoldChange
FC ≥ 1
0.5 ≤ FC < 1
0 < FC < 0.5
-0.5 < FC <0
-1 < FC ≤ -0.5
FC ≤ -1
F
RNA-seq
Spearman coefficient
All
DE
IFNα
IL-12
aNK1.1
IL-2
IL-15
ATAC-seq
All
DA
G
10 kb
Unstim
aNK1.1
Ly49H- Nur77all
Ly49H+ Nur77low
Ly49H+ Nur77high
Crtam
log(TPM + 1)
Unstim.
aNK1.1
Ly49H- Nur77all
Ly49H+ Nur77low
Ly49H+ Nur77high

Figure 3

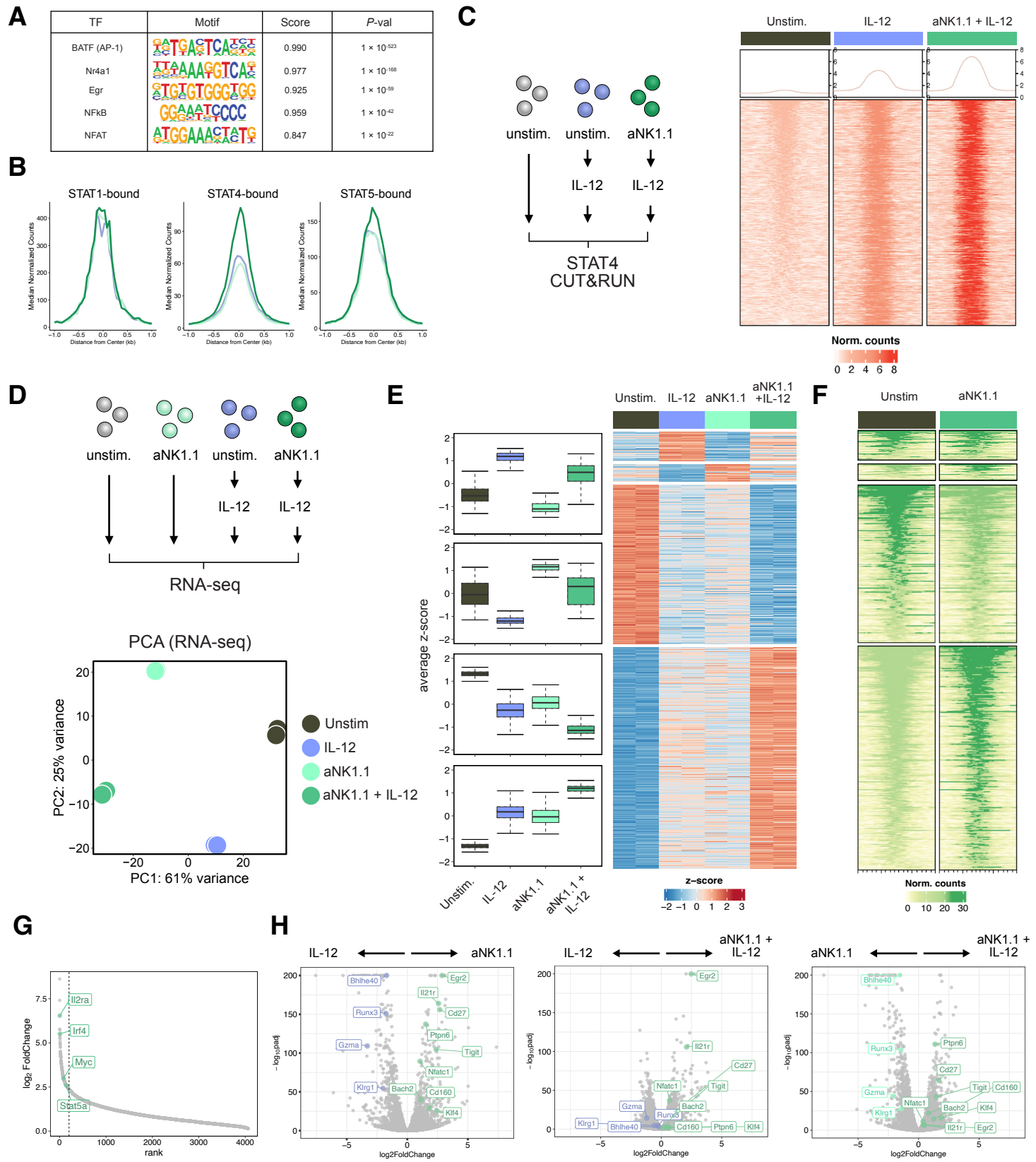
A
TF
Motif
Score
P-val
BATF (AP-1)
0.990
1 × 10-523
Nr4a1
0.977
1 × 10-168
Egr
0.925
1 × 10-59
NFkB
0.959
1 × 10-42
NFAT
0.847
1 × 10-22
B
STAT1-bound
STAT4-bound
STAT5-bound
Median Normalized Counts
Distance from Center (kb)
C
unstim.
unstim.
aNK1.1
IL-12
IL-12
STAT4
CUT&RUN
Unstim.
IL-12
aNK1.1 + IL-12
Norm. counts
D
unstim.
aNK1.1
unstim.
aNK1.1
IL-12
IL-12
RNA-seq
PCA (RNA-seq)
PC2: 25% variance
PC1: 61% variance
Unstim
IL-12
aNK1.1
aNK1.1 + IL-12
E
average z-score
Unstim.
IL-12
aNK1.1
aNK1.1 +IL-12
z-score
F
Unstim
aNK1.1
Norm. counts
G
log2 FoldChange
rank
Il2ra
Irf4
Myc
Stat5a
H
IL-12
aNK1.1
aNK1.1 + IL-12
log2FoldChange
Bhlhe40
Runx3
Gzma
Klrg1
Egr2
Il21r
Cd27
Ptpn6
Tigit
Nfatc1
Bach2
Cd160
Klf4

Figure 4

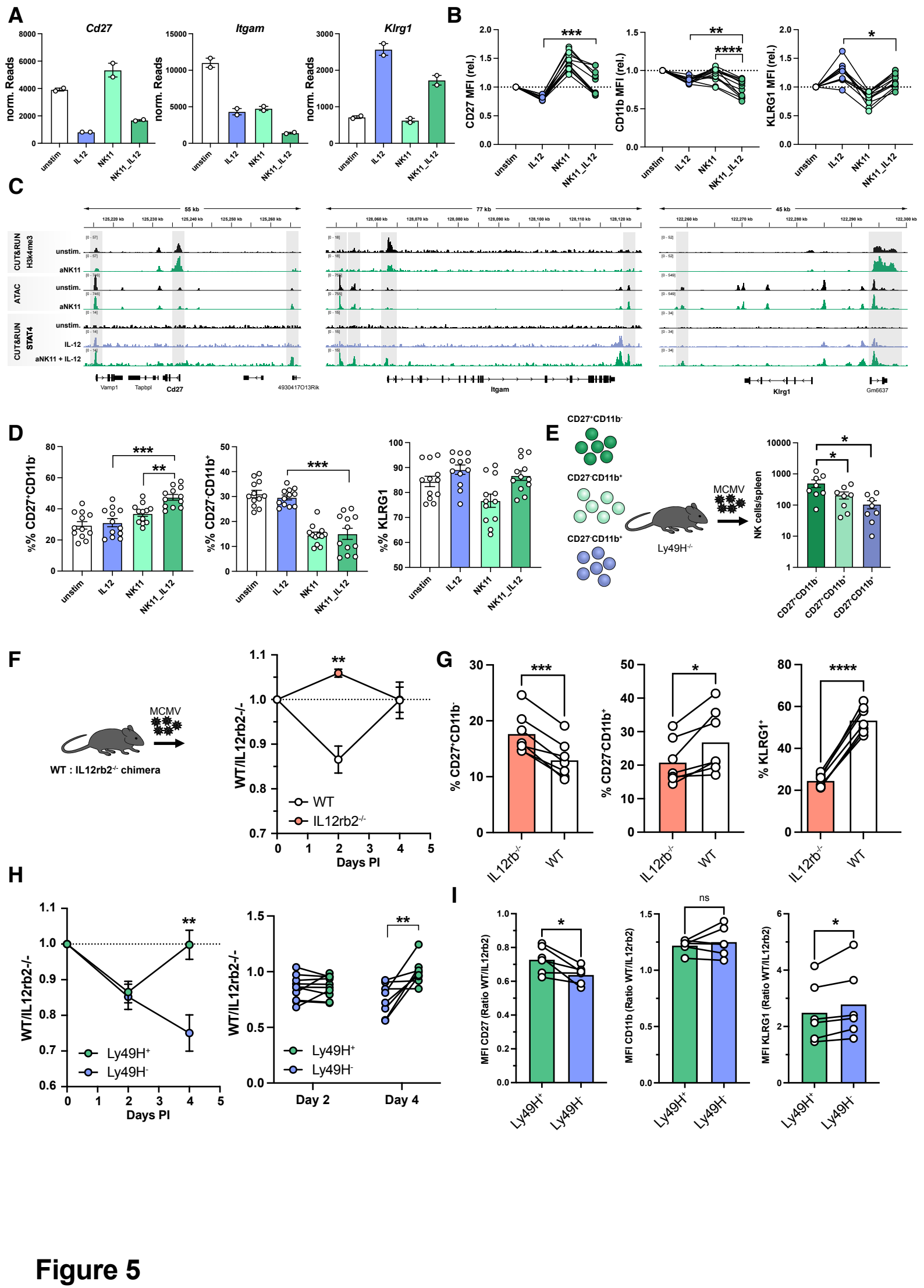
A
Cd27
Itgam
Klrg1
norm. Reads
unstim
IL12
NK11
NK11_IL12
B
CD27 MFI (rel.)
CD11b MFI (rel.)
KLRG1 MFI (rel.)
C
55 kb
77 kb
45 kb
CUT&RUN H3k4me3
ATAC
CUT&RUN STAT4
unstim.
aNK11
IL-12
aNK11 + IL-12
Vamp1
Tapbpl
Cd27
4930417O13Rik
Itgam
Klrg1
Gm6637
D
%% CD27+CD11b-
%% CD27-CD11b+
%% KLRG1
E
CD27+CD11b-
CD27-CD11b+
CD27-CD11b+
MCMV
Ly49H-/-
NK cells/spleen
F
MCMV
WT : IL12rb2-/- chimera
WT/IL12rb2-/-
WT
IL12rb2-/-
Days PI
G
% CD27+CD11b-
% CD27-CD11b+
% KLRG1+
IL12rb-/-
WT
H
WT/IL12rb2-/-
Ly49H+
Ly49H-
Days PI
Day 2
Day 4
I
MFI CD27 (Ratio WT/IL12rb2)
MFI CD11b (Ratio WT/IL12rb2)
MFI KLRG1 (Ratio WT/IL12rb2)
ns

Figure 5

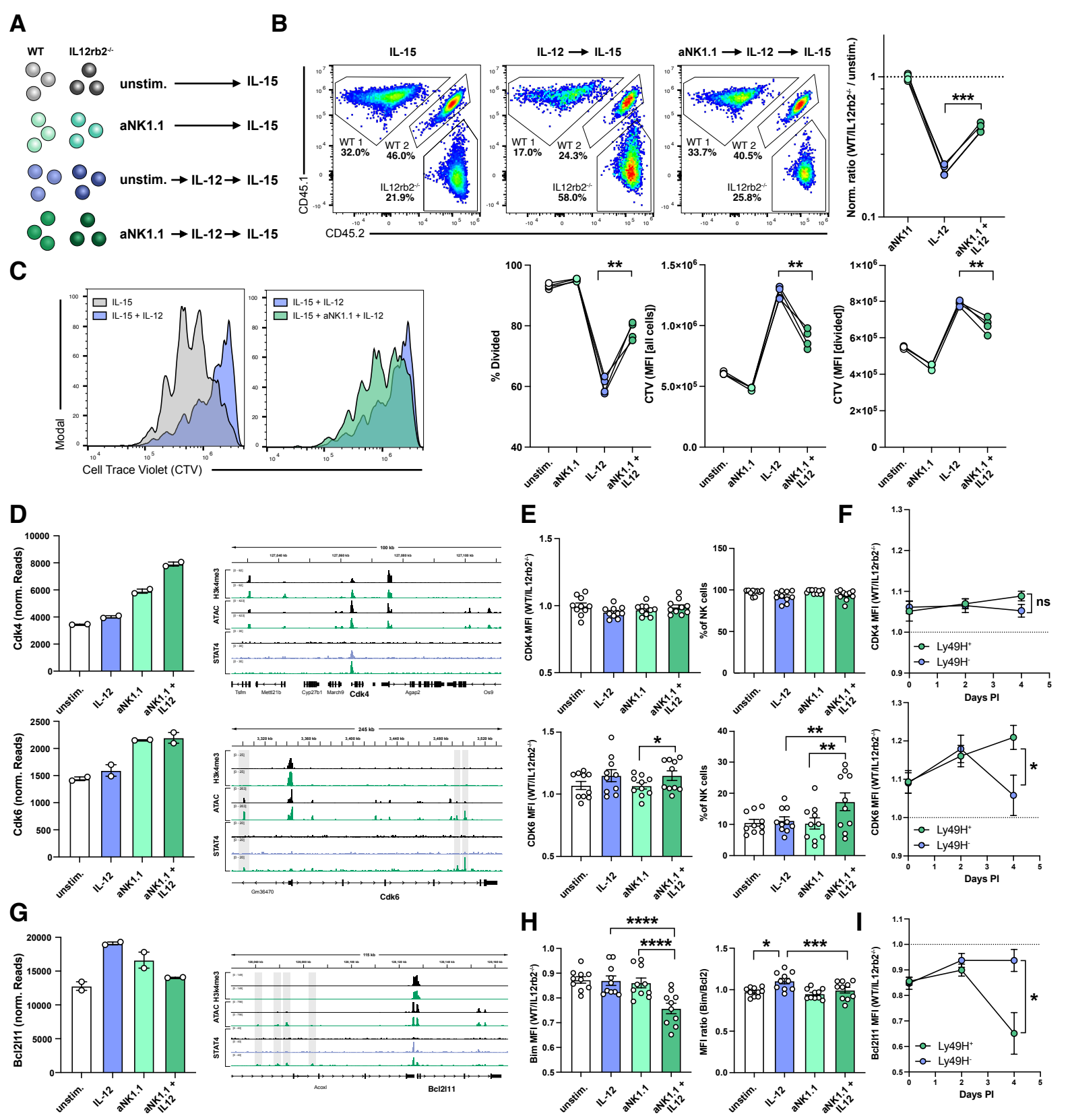
A
WT
IL12rb2-/-
unstim. → IL-15
aNK1.1 → IL-15
unstim. → IL-12 → IL-15
aNK1.1 → IL-12 → IL-15
B
IL-15
IL-12 → IL-15
aNK1.1 → IL-12 → IL-15
WT 1 32.0%
WT 2 46.0%
IL12rb2-/- 21.9%
WT 1 17.0%
WT 2 24.3%
IL12rb2-/- 58.0%
WT 1 33.7%
WT 2 40.5%
IL12rb2-/- 25.8%
CD45.1
CD45.2
Norm. ratio (WT/IL12rb2-/- / unstim.)
***
aNK11
IL-12
aNK1.1 + IL12
C
IL-15
IL-15 + IL-12
IL-15 + aNK1.1 + IL-12
Modal
Cell Trace Violet (CTV)
% Divided
CTV (MFI [all cells])
CTV (MFI [divided])
**
unstim.
aNK1.1
IL-12
aNK1.1 + IL12
D
Cdk4 (norm. Reads)
Cdk6 (norm. Reads)
H3k4me3
ATAC
STAT4
Cdk4
Cdk6
E
CDK4 MFI (WT/IL12rb2-/-)
CDK6 MFI (WT/IL12rb2-/-)
%of NK cells
F
CDK4 MFI (WT/IL12rb2-/-)
CDK6 MFI (WT/IL12rb2-/-)
Ly49H+
Ly49H-
Days PI
ns
G
Bcl2l11 (norm. Reads)
Bcl2l11
H
Bim MFI (WT/IL12rb2-/-)
MFI ratio (Bim/Bcl2)
****
***
I
Bcl2l11 MFI (WT/IL12rb2-/-)

Figure 6

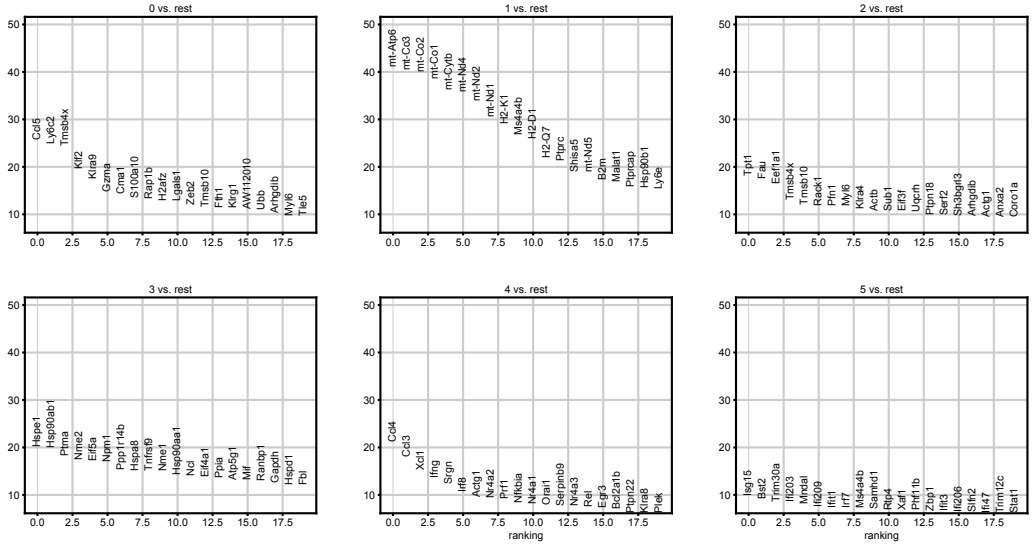
0 vs. rest
Ccl5
Ly6c2
Tmsb4x
Klf2
Klra9
Gzma
Cma1
S100a10
Rap1b
H2afz
Lgals1
Zeb2
Tmsb10
Fth1
Klrg1
AW112010
Ubb
Arhgdib
Myl6
Tle5
1 vs. rest
mt-Atp6
mt-Co3
mt-Co2
mt-Co1
mt-Cytb
mt-Nd4
mt-Nd2
mt-Nd1
H2-K1
Ms4a4b
H2-D1
H2-Q7
Ptprc
Shisa5
mt-Nd5
B2m
Malat1
Ptprcap
Hsp90b1
Ly6e
2 vs. rest
Tpt1
Fau
Eef1a1
Tmsb4x
Tmsb10
Rack1
Pfn1
Myl6
Klra4
Actb
Sub1
Eif3f
Uqcrh
Ptpn18
Serf2
Sh3bgrl3
Arhgdib
Actg1
Anxa2
Coro1a
3 vs. rest
Hspe1
Hsp90ab1
Ptma
Nme2
Eif5a
Npm1
Ppp1r14b
Hspa8
Tnfrsf9
Nme1
Hsp90aa1
Ncl
Eif4a1
Ppia
Atp5g1
Mif
Ranbp1
Gapdh
Hspd1
Fbl
4 vs. rest
Ccl4
Ccl3
Xcl1
Ifng
Srgn
Irf8
Actg1
Nr4a2
Prf1
Nfkbia
Nr4a1
Olfr1
Serpinb9
Nr4a3
Rel
Egr3
Bcl2a1b
Ptpn22
Klra8
Plek
ranking
5 vs. rest
Isg15
Bst2
Tnfrsf9
Ifi203
Mndal
Ifi204
Irf7
Ms4a4b
Samd1
Rtp4
Xaf1
Phf11b
Zbp1
Ifi213
Ifi206
Slfn2
Ifi47
Trim12c
Stat1
ranking

Figure S1

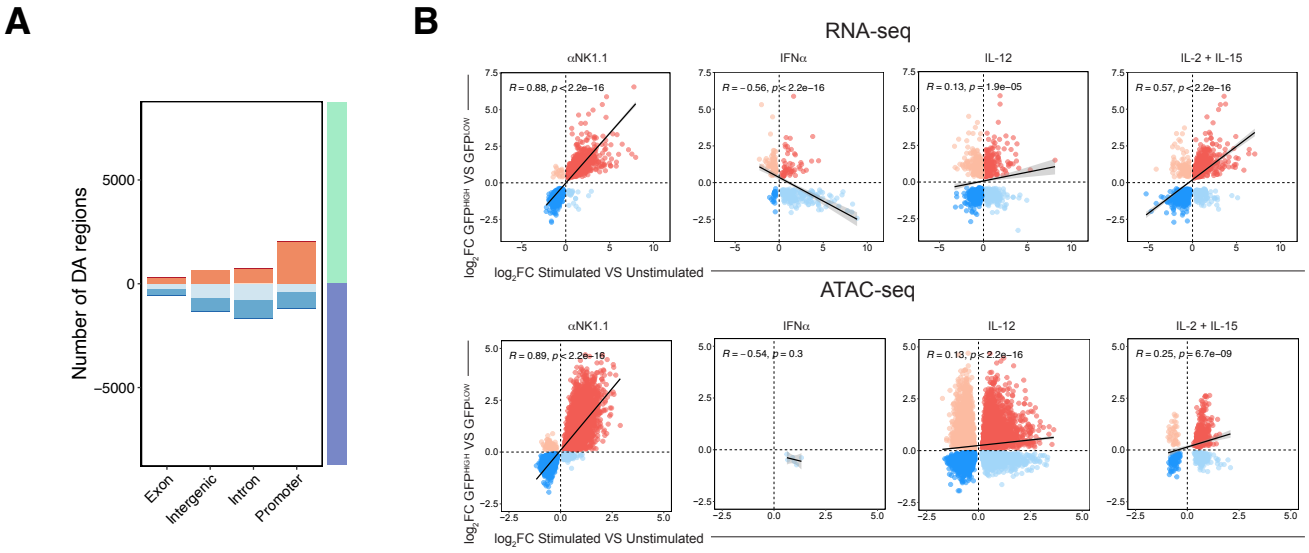
A
Number of DA regions
5000
0
−5000
Exon
Intergenic
Intron
Promoter
B
RNA-seq
αNK1.1
IFNα
IL-12
IL-2 + IL-15
R = 0.88, p < 2.2e−16
R = −0.56, p < 2.2e−16
R = 0.13, p = 1.9e−05
R = 0.57, p < 2.2e−16
log2FC GFPHIGH VS GFPLOW
log2FC Stimulated VS Unstimulated
ATAC-seq
αNK1.1
IFNα
IL-12
IL-2 + IL-15
R = 0.89, p < 2.2e−16
R = −0.54, p = 0.3
R = 0.13, p < 2.2e−16
R = 0.25, p = 6.7e−09
log2FC GFPHIGH VS GFPLOW
log2FC Stimulated VS Unstimulated

Figure S2

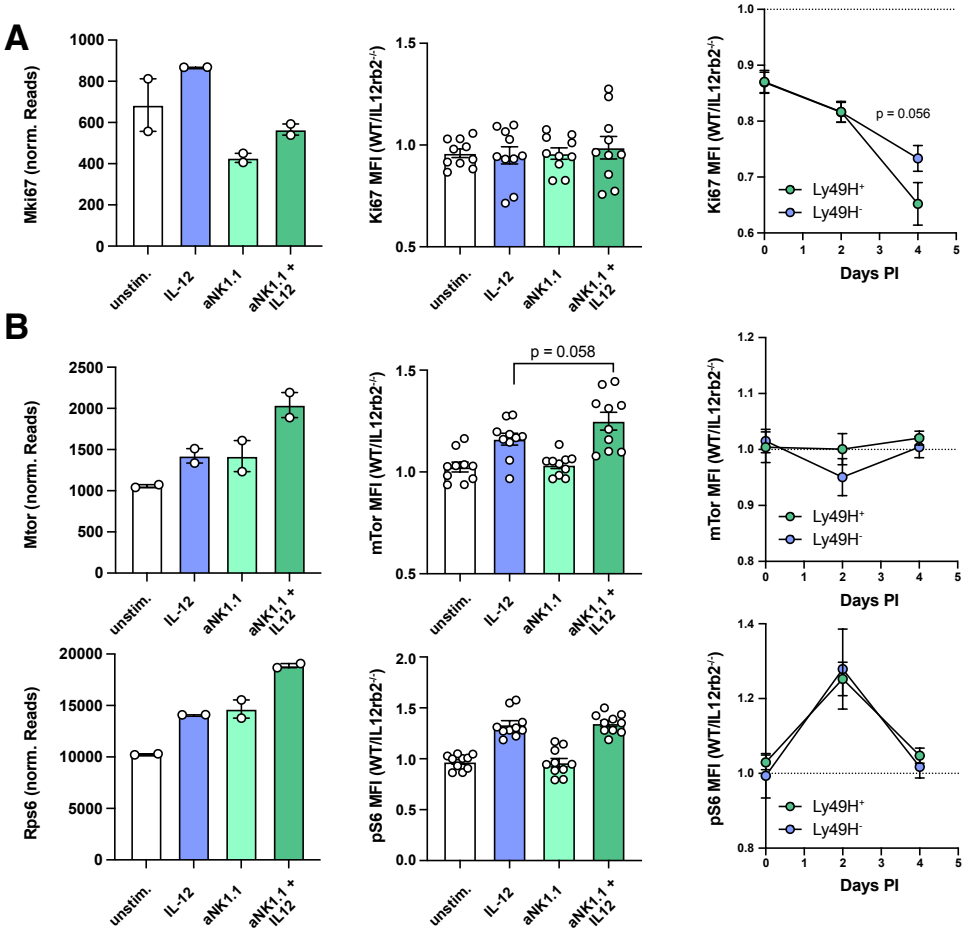
A
Mki67 (norm. Reads)
Ki67 MFI (WT/IL12rb2-/-)
Ki67 MFI (WT/IL12rb2-/-)
p = 0.056
Ly49H+
Ly49H-
Days PI
unstim.
IL-12
aNK1.1
aNK1.1 + IL12
B
Mtor (norm. Reads)
mTor MFI (WT/IL12rb2-/-)
p = 0.058
mTor MFI (WT/IL12rb2-/-)
Rps6 (norm. Reads)
pS6 MFI (WT/IL12rb2-/-)
pS6 MFI (WT/IL12rb2-/-)

Figure S3